M

8820

NASA Technical Memorandum

NASA TM-86542

CALIBRATION OF THE ISEE PLASMA COMPOSITION EXPERIMENT

By C. R. Baugher, R. C. Olsen, and D. L. Reasoner

Space Science Laboratory

March 1986

(NASA-TM-86542) CALIBRATION OF THE ISEE PLASMA COMPOSITION EXPERIMENT (NASA) 60 p HC A04/MF A01 CSCL 22A

N86-26348

Unclas

G3/12 43423

National Aeronautics and Space Administration

George C. Marshall Space Flight Center

MSFC - Form 3190 (Rev. May 1983)

TECHNICAL REPORT STANDARD TITLE PAGE

1. REPORT NO. NASA TM -86542	2. GOVERNMENT ACCESSION NO.	3. RECIPIENT'S CATALOG NO.
4. TITLE AND SUBTITLE Calibration of the ISEE Plasma Composition Experiment		5. REPORT DATE March 1986
		6. PERFORMING ORGANIZATION CODE
7. AUTHOR(S) C. R. Baugher, R. C. Olsen,* and D. L. Reasoner		8. PERFORMING ORGANIZATION REPORT #
9. PERFORMING ORGANIZATION NAME AND ADDRESS George C. Marshall Space Flight Center Marshall Space Flight Center, Alabama 35812		10. WORK UNIT NO.
		11. CONTRACT OR GRANT NO.
12. SPONSORING AGENCY NAME AND ADDRESS National Aeronautics and Space Administration Washington, D.C. 20546		13. TYPE OF REPORT & PERIOD COVERED Technical Memorandum
		14. SPONSORING AGENCY CODE

15. SUPPLEMENTARY NOTES

Prepared by Space Science Laboratory, Science and Engineering Directorate.

* Physics Department, The University of Alabama in Huntsville, Huntsville, AL 35899.

16. ABSTRACT

The Plasma Composition experiment on the ISEE-1 satellite was designed to measure ions from 1 to 16 amu, at energies from near zero to 16 keV. The two nearly identical flight instruments were calibrated by means of preflight laboratory tests and in-flight data comparisons. This document presents most of the details of those efforts, with special emphasis on the low energy (0-100 eV) portion of the instrument response. The analysis of the instrument includes a ray-tracing calculation, which follows an ensemble of test particles through the detector.

17. KEY WORDS Instrument calibration Thermal plasma	18. DISTRIBUTION STATEMENT C. R. Baugher Unclassified — Unlimited

19. SECURITY CLASSIF. (of this report) Unclassified	20. SECURITY CLASSIF. (of this page) Unclassified	21. NO. OF PAGES 62	22. PRICE NTIS

MSFC - Form 3292 (May 1969)

For sale by National Technical Information Service, Springfield, Virginia 22151

ACKNOWLEDGMENTS

The details of the Head A calibration, which differed from that of Head B, are based on a manuscript produced by E. Hertzberg, then at Lockheed, Palo Alto. Critical comments were added by E. G. Shelley, W. K. Petersen, and the rest of the Lockheed research staff.

TABLE OF CONTENTS

		Page
I.	APERTURE POINTING AND APERTURE ACCEPTANCE ANGLE	1
II.	INTER-SENSOR GAINS	9
III.	DENSITY CALCULATIONS	15
IV.	ENERGY PASSBAND-BIAS CHECKS	20
V.	HEAD A CALIBRATION	21
VI.	RAY TRACING	28
APPENDIX A -	DEFINITIONS AND PHYSICAL CONSTANTS	39
APPENDIX B -	PARTICLE "SCORECARD" MATRICES	41
APPENDIX C -	COMPUTATION OF GEOMETRIC FACTOR (G.F.) FROM THE DATA	47
APPENDIX D -	TRAJECTORY THROUGH PLATES	49
APPENDIX E -	EFFECTS OF REFRACTION AT ANALYZER ENTRANCE AND EXIT	51
REFERENCES		55

LIST OF ILLUSTRATIONS

Figure	Title	Page
1.	ISEE-1 satellite with principal appendages	1
2.	Synopsis of the ISEE-1 satellite orbit	2
3.	Definition of satellite coordinate system	3
4a.	PCE diagram, side view, with emphasis on electrostatic analyzer	4
4b.	PCE diagram, side view and top view, with emphasis on optical path dimensions	4
4c.	PCE diagram, energy detector apertures	5
5.	Detector angular response calibration, Head B, energy detector 2, and model	7
6.	Detector angular response calibration, Head B, energy detectors 1 and 2	8
7.	Summary of relative detector efficiencies for Head B, based on pre-flight calibration data	9
8a.	Flight data from Head B, comparing data from energy detectors 1 and 2	10
8b.	Flight data from Head B, comparing data from the mass detector at low gain and high gain	10
9.	Summary of relative detector efficiencies for Head B, as modified to include results from analysis of flight data, early in the detector life	11
10a.	Pitch angle distributions for H+, showing the ratio of the fluxes for the mass detector and energy detector 2	12
10b.	Pitch angle distributions for Head B, H+, ED2 and MD	12
10c.	Pitch angle distributions for Head B, H+, ED2 and MD	13
11.	Summary of relative detector efficiencies for Head B, based on flight data, late in detector life	14
12.	Effects of velocity and temperature on the density calculation	16
13.	Comparison of plasmasphere density profiles obtained from the PCE and the plasma wave instrument	18
14.	Characteristics of the electrostatic analyzer response in the RPA mode, Head B, flight data	20

LIST OF ILLUSTRATIONS (Continued)

Figure	Title	Page
15.	Characteristics of the electrostatic analyzer response in the RPA mode, Head A, ED2 and MD, laboratory	22
16.	Characteristics of the electrostatic analyzer response in the RPA mode, Head B, ED2 and MD, laboratory	22
17.	Analyzer constant for Head A, energy detector (ED)	24
18.	Analyzer constant for Head A, mass detector (MD)	25
19.	Analyzer constant for Head B, energy detector (ED)	26
20.	Analyzer constant for Head B, mass detector (MD)	27
21.	Characteristics fo the electrostatic analyzer response in the RPA mode, Head B, ED1, laboratory	28
22.	PCE optical path, ray tracing version	29
23.	Electrostatic analyzer plates	29
24.	Details of electrostatic analyzer plates	30
25.	Probability response as a function of theta 1	45
26.	Probability response as a function of theta 2	46

LIST OF TABLES

Table	Title	Page
1.	Gain Comparisons Head B	14
2.	Effective Area Calibration	17
3.	Satellite Potential Effects on Current to an RPA	19
4.	Geometric Factors	19

TECHNICAL MEMORANDUM

CALIBRATION OF THE ISEE PLASMA COMPOSITION EXPERIMENT

I. APERTURE POINTING AND APERTURE ACCEPTANCE ANGLE

Figure 1 is a drawing of the ISEE spacecraft. The spacecraft is a 16-sided polygon with booms. The +Y-axis is along the ACS extention and emerges from the spacecraft body between Faces 1 and 16. The +X-axis emerges from the spacecraft body between Faces 12 and 13. The Plasma Composition Experiment is actually two independent and almost identical instruments; Head A and Head B. Both heads are in the same face mounted one above the other. Head A is on top and Head B is mounted below but is upside down with respect to Head A. Although each head looks radially outward, they are canted slightly such that they do not look perpendicular to the spacecraft spin axis (+Z). The center line of Head A is directed 95 deg from the spin axis, the center line of Head B is directed 85 deg from the spin axis.

The ISEE orbit is inclined 30 deg to the Earth's equator. The spacecraft's spin axis is actively controlled to within about a degree of perpendicular to the ecliptic plane. Hence, the two heads are looking approximately in the ecliptic plane, but the relation of the pointing of the heads with respect to the velocity vector is more complicated. Figure 2 is a predicted plot of the angle between the perpendicular to the spin axis and the velocity vector as a function of distance from the center of the Earth during the first four years of the spacecraft's lifetime.

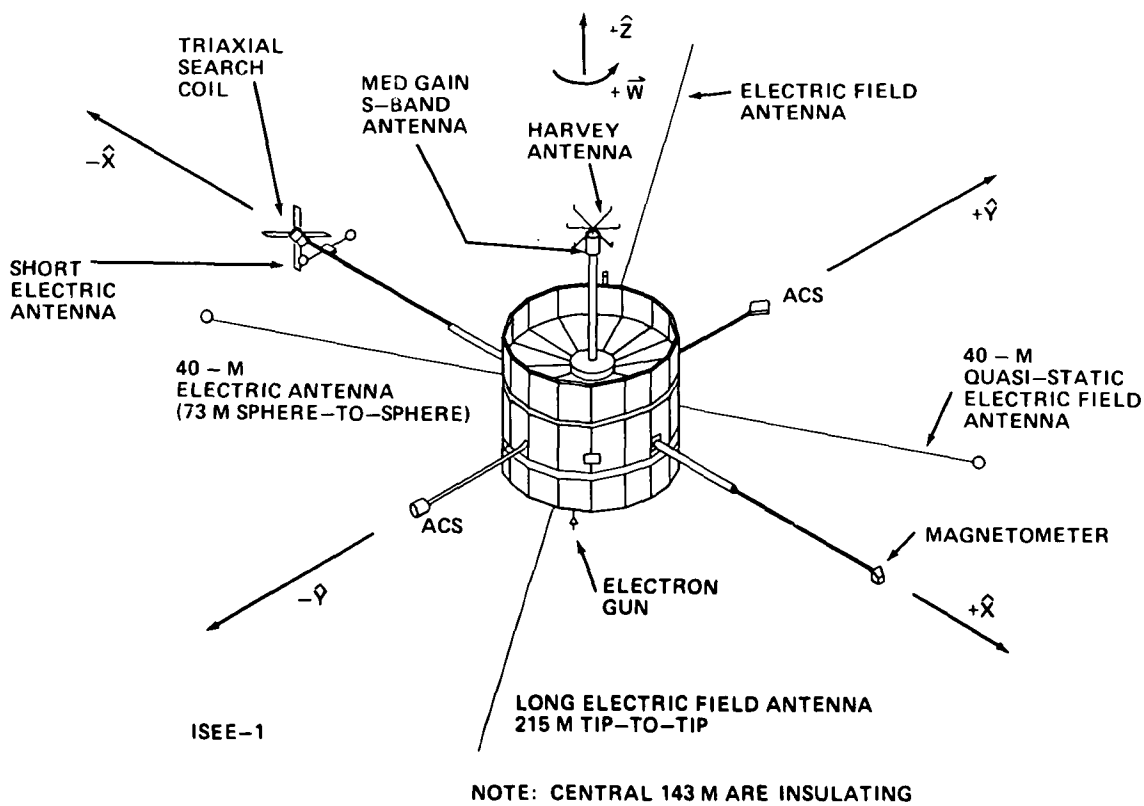

Figure 1. ISEE-1 satellite with principal appendages.

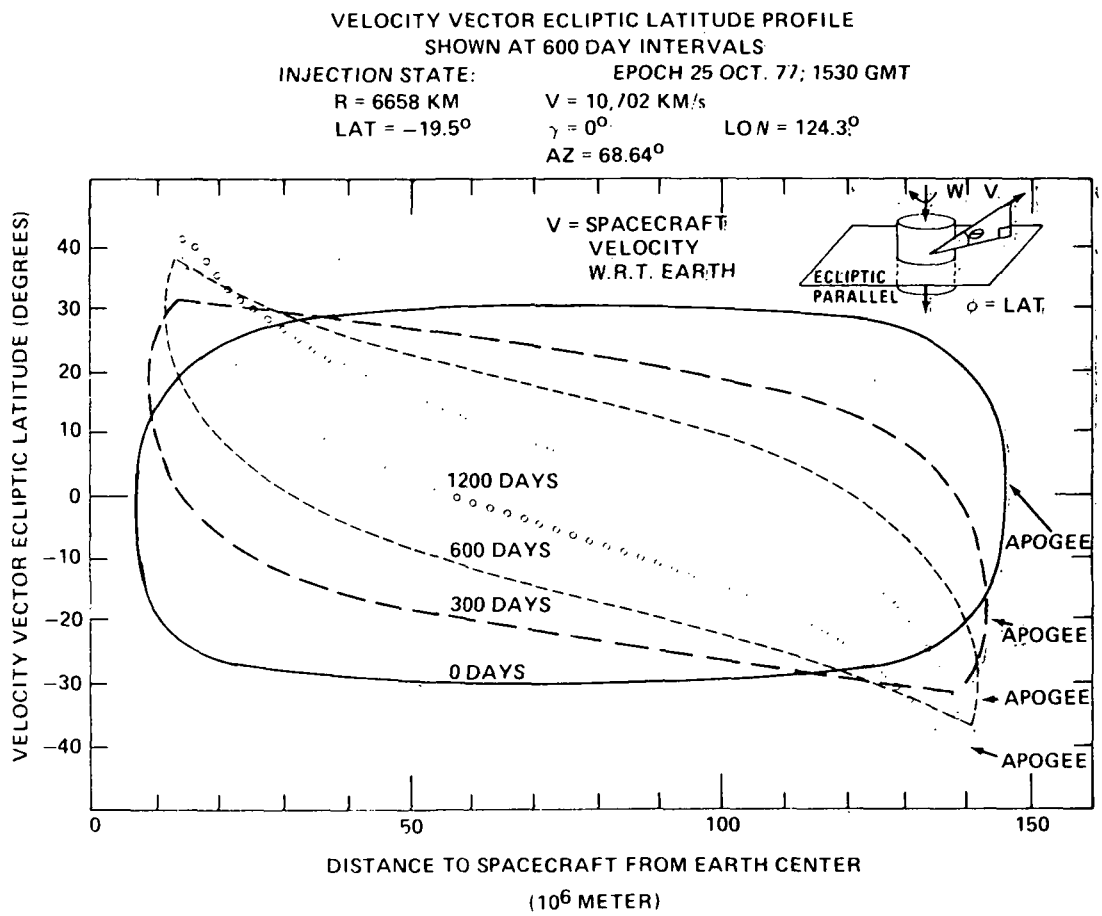

Figure 2. Synopsis of the ISEE-1 satellite orbit.

Figure 3 is a diagram of the coordinate system used to describe the geometry of the experiment. The various angles are defined as follows:

θ_S = THETAS = the angle between the Z-axis and the velocity axis

θ_D = THETAD = the angle between the Z-axis and the center of the detector aperture

ϕ_D = PHID = the angle between the X-axis and the center of the detector aperture

NOTE: The coordinate system is defined such that the spacecraft velocity lies in the X-Z plane.

α = ALPHA = the azimuthial acceptance angle

β = BETA = the polar acceptance angle .

Each head of the Plasma Composition Experiment consists of a rectangular aperture (9.4 x 2.2 cm) which is mounted flush with the spacecraft surface. Following the aperture is a collimating section which, ideally, establishes the angular response characteristics of the instrument purely by its geometry. The aperture acceptance angle is nominally α = 12 deg, β = 45 deg.

Following this section is a region of electrostatic acceleration in which the incoming ions are accelerated to approximately 3000 electron volts. Subsequently, this

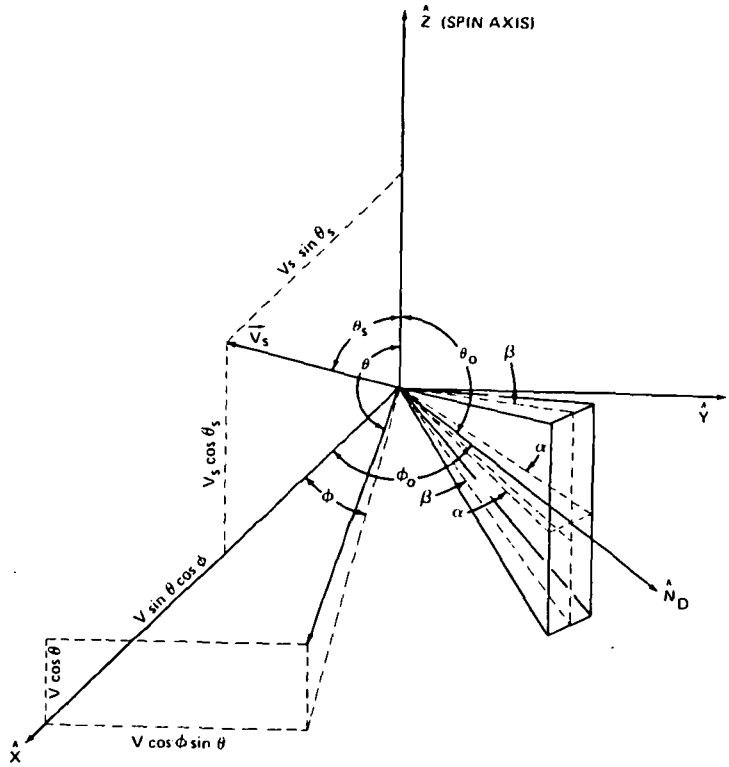

Figure 3. Definition of satellite coordinate system.

ion beam is energy analyzed and split. A portion is detected by channel electron multipliers and a portion is input to the mass spectrometer, mass analyzed, and then detected by a Johnston multiplier.

Two independent attempts have been made to analytically model the instrument. The first is a simple first order analysis restricted to an analysis of the collimating section of the instrument using a Maxwellian input. The second method was an elegant modeling of the trajectories of individual particles through the fields of the electrostatic analyzer section of the instrument. The first order approach is presented first, followed by the Head A calibration results, and then the ray tracing effort.

To a first approximation, it can be assumed that once the incoming ions are accelerated by the 3000 V potential, they "fly straight" through the subsequent analyzers and detectors. This assumption has the effect of "imaging" the detector after the energy analyzer and the detector after the mass analyzer forward to the plane at which the ions are accelerated. The resulting configuration is shown in Figure 4(a,b,c). (See also Figure 22 in the Ray Tracing section.) Figure 4a is a vertical slice through the instrument in the plane of the Z-axis and the detector normal. The aperture is to the left (0.0944 m); the detectors are arrayed to the right and labeled MD for the mass analyzer detector, ED2 for the high gain energy analyzer detector, and ED1 for the low gain energy analyzer detector. It is to be noted that the switch between high and low gain in the energy analyzer detector is accomplished by actually physically switching between a pair of detectors with different effective areas; whereas the change in gain at the mass analyzer detector is accomplished by changing the bias on the plates of a single detector.

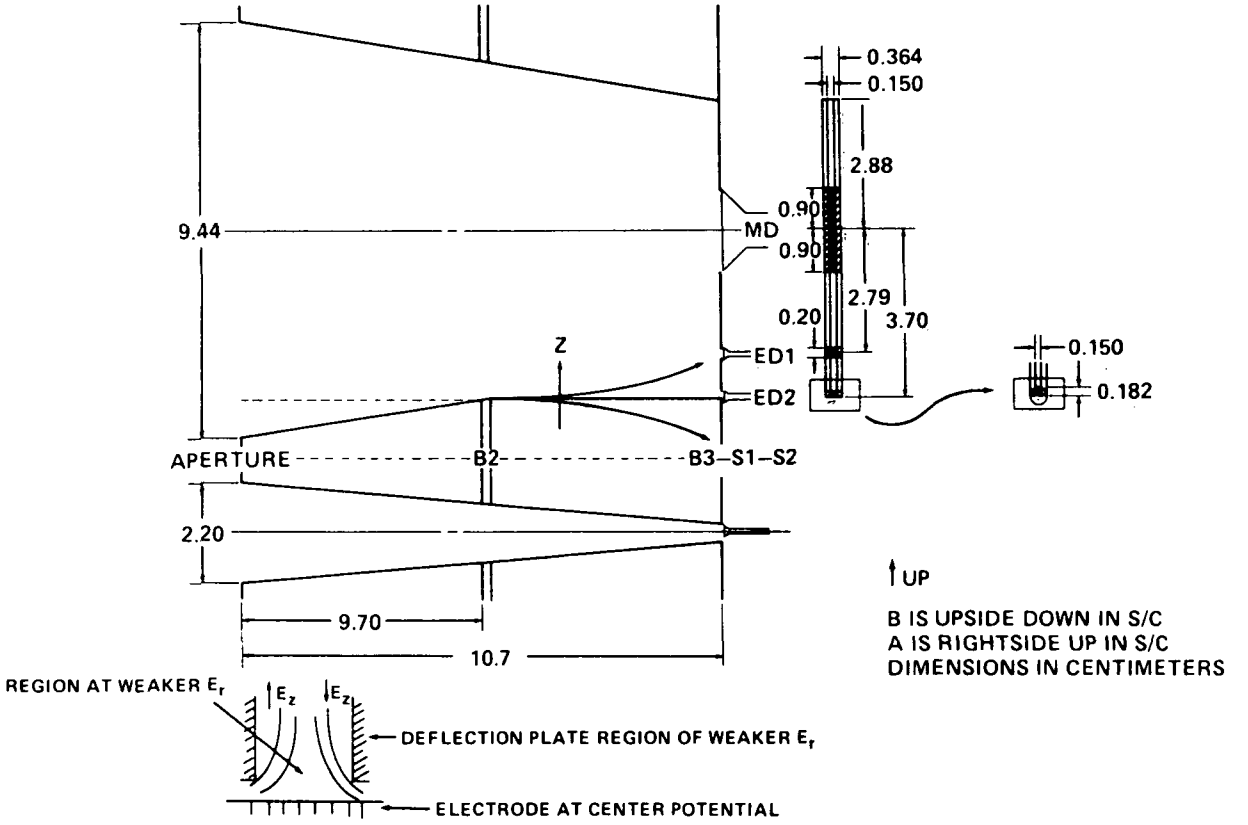

Figure 4a. PCE diagram, side view, with emphasis on electrostatic analyzer.

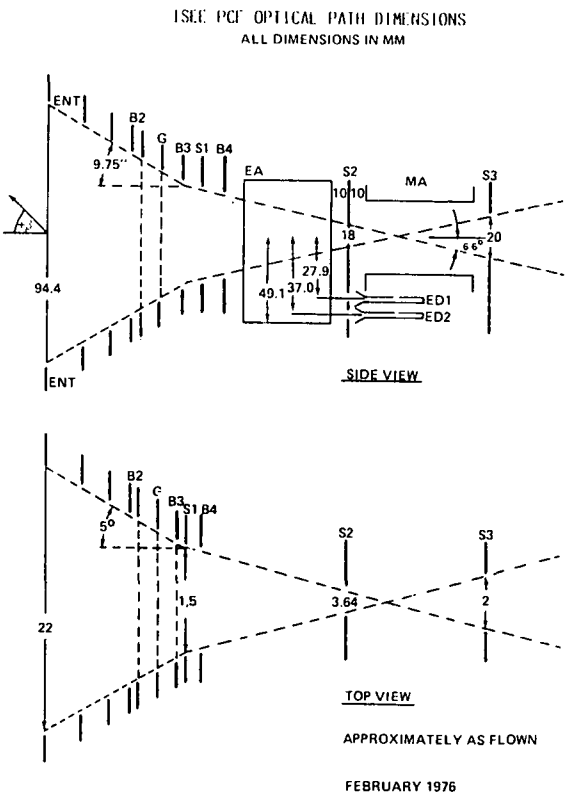

Figure 4b. PCE diagram, side view and top view, with emphasis on optical path dimensions.

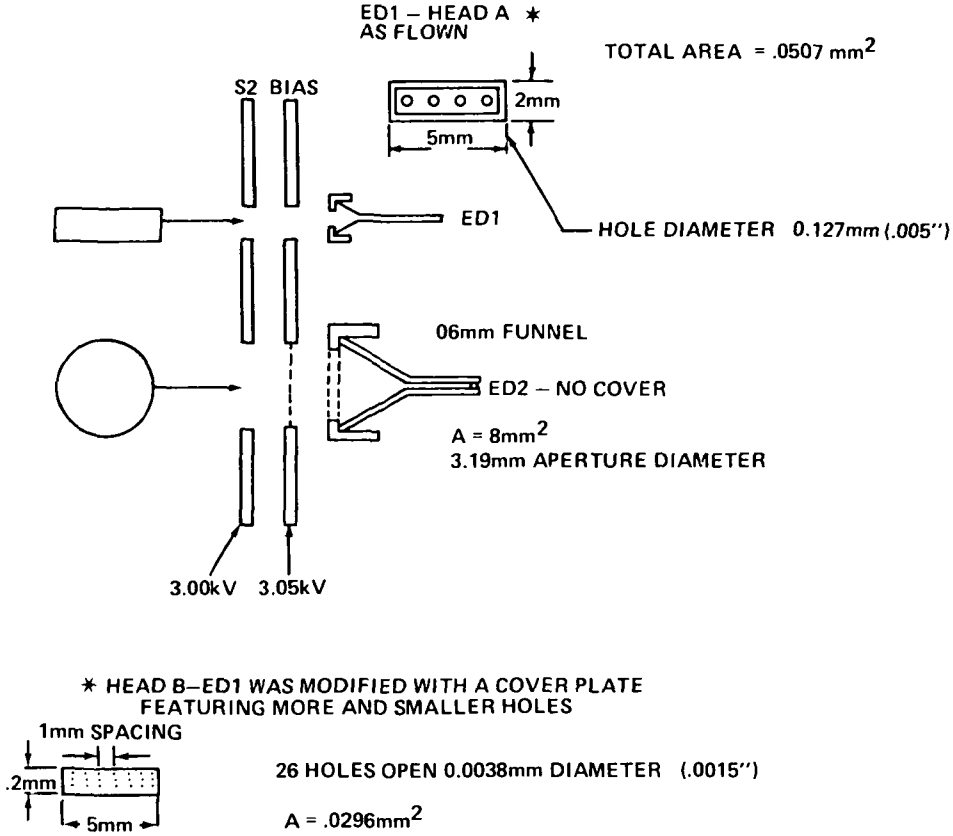

Figure 4c. PCE diagram, energy detector apertures.

Figure 4: The instrument consists of:

1) Collimater

2) RPA:

   a) Ground grid

   b) Retarding grid

   c) Ground grid

3) Pre-acceleration region – 3 kV (actually varied in 25 V steps around -2950 V – see Energy Passband Section)

4) ESA

5) Magnets

Note the relative placement of the three detectors. MD is in the most advantageous position, directly centered behind the limiting aperture opening. The angle subtended between the center of this detector and the aperture (angle β) is approximately 95 deg with the center line of this angle down the "bore-sight" of the instrument. ED1 is offset from the center line. It can be calculated that the total angle (β) subtended between ED1 and the aperture is still approximately 45 deg but from the geometrical considerations, the center line of the angle has been shifted approximately 12 deg off the center line of the instrument.

ED2 is in the most compromised location. Its surface is actually partially masked from the aperture by structure internal to the instrument. The total angle subtended by the aperture at the center of this detector remains close to 45 deg (β = 43 deg is actually calculated), but the center line of this detector's viewing is shifted 16.5 deg above the instrument's center line.

Two further complications should be considered. The first is the angle of incidence of the particles when they strike the detector. Particles which enter the aperture at the upper edge and strike ED2 and are counted are arriving at the detector at a 38 deg angle of incidence. Particles which enter the lower edge of the aperture strike the detector at near normal incidence. The second effect is due to the finite size of the detectors. Each point on the detector face actually has a slightly different viewing angle through the aperture. This effect would be most pronounced for MD since it is physically the largest, although it could be argued that it might also influence the energy detectors.

To check these two effects, a calculation was made in which the face of each detector was subdivided into a square array of elements. The angle subtended between each element and the aperture was calculated and the response of this "elemental," limited aperture to a drifting Maxwellian was calculated. The results from each of the elements were then summed. The calculation was repeated for different THETAD angles with PHID = 0 to form a response versus angle curve. Of the two effects mentioned, only the cosine effect was significant, and this only for ED2. All detectors were physically small enough to be considered, for all practical purposes, point detectors. The results of the calculation for ED2 are shown in Figure 5. Three of the curves in this plot are calculated β response curves, the fourth curve is calibration data taken utilizing a 19 eV beam for Head B.

Two of the calculations were made at high Mach numbers to simulate the calibration beam. The third curve was calculated at a low Mach number to demonstrate that the effects which are being discussed, and even the relative importance of the absolute pointing, tend to lose significance at the lower Mach numbers.

It is interesting to note that although the center of the full-width-half-max of the curve is indeed centered approximately 16 deg off the center line of the instrument (90 deg point on the plot), the ED2 response function tends to be higher near the center line than away from it. To first order, this phenomenon would tend to shift the ED2 average response toward the instrument's center line by a few degrees, bringing it more into line with ED1, where the effect of an asymmetric peaking was less pronounced.

All of the above is valid only insofar as it is supported by calibration data; which in the case ED2, Head B, it was not. The calibration curve on the plot shows that the measured response of the instrument appeared to be down substantially near the instrument center line. This points to the possibility that the detector is actually

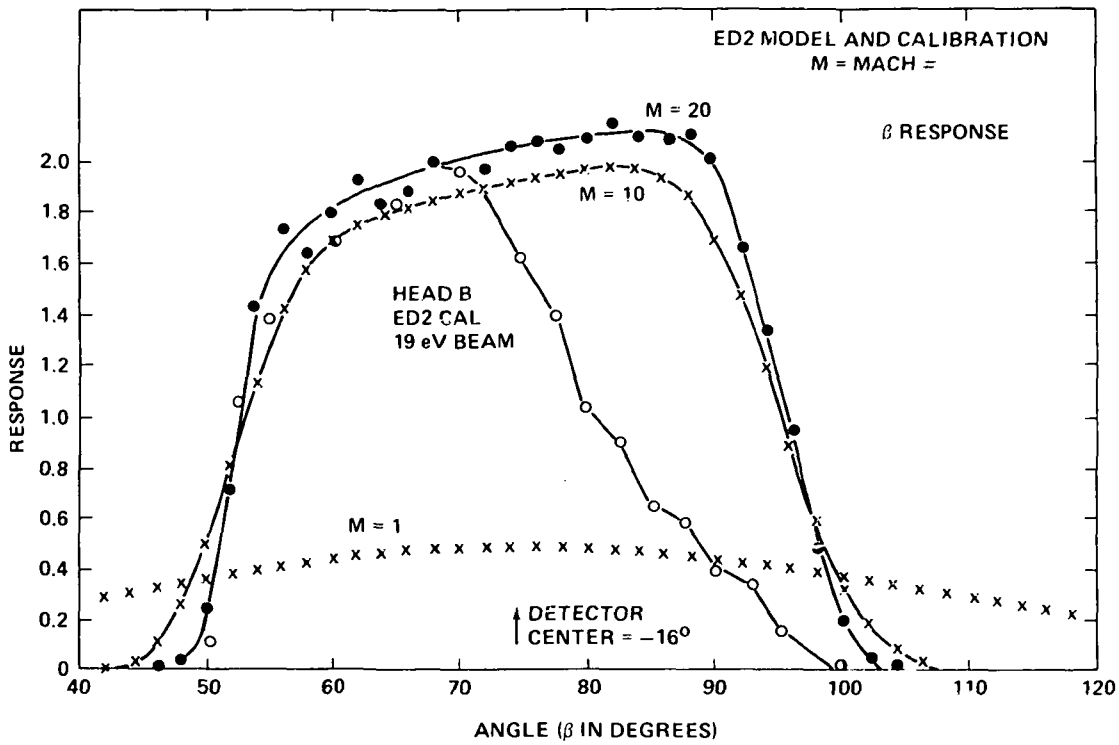

Figure 5. Detector angular response calibration, Head B, energy detector 2, and model.

cut off from the aperture by the internal structure by more than was anticipated or that strong fields inside the collimating section are playing an important role in determining the ED2 angular response and pointing. The center of this measured response function is 29 deg from the instrument center line and the FWHM dimension is 28 deg.

The calibration measurement for ED1 was slightly better and is shown in Figure 6. This plot contains both data from ED1 and ED2. The FWHM dimension of the ED1 curve is 38 deg and the center line of the response is at 11 deg from the instrument center line. The data of Figure 6 were taken for Head B of the Plasma Composition Experiment and are essentially the sum-total of the preflight, low-energy calibration data.

The foregoing first order effort to model the forward part of the ISEE instrument was an attempt to establish an analytic base line from which to judge the performance of the instrument vis-a-vis its design parameters and then extrapolate to a response for the very low energy Maxwellian plasma of the plasmasphere. While it was intellectually interesting, it probably adds only little to our understanding of the instrument. If the problem in the comparison with the calibration data is geometrical, that is, if ED2 is shadowed more than intended by internal surfaces, then the geometry of the model could be adjusted until the calibration data were reproduced and a valid extrapolation could be accomplished. If, on the other hand, the problem is one of stray fields in the energy analyzer, then accurate modeling and extrapolation is unrealistic. (A. Ghielmetti suggested there should be a deflection in the z direction due to fringe fields in the energy analyzer, and E. Shelley adds there may be a z component to the field in the edge regions of the RPA-Accelerator section.)

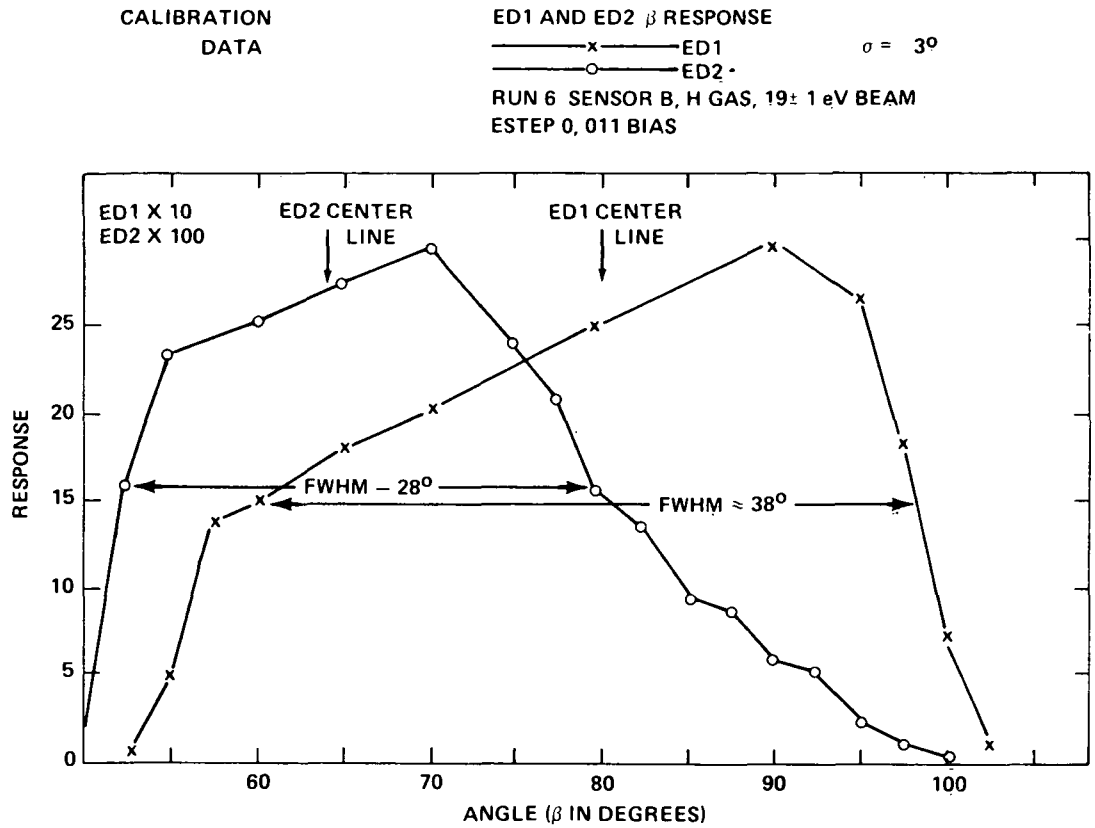

Figure 6. Detector angular response calibration, Head B, energy detectors 1 and 2.

Note that the calibration data were taken at 19 electron volts. With lower energy plasma the effects of strong fields would be magnified in an unknown fashion. Finally, there is the possibility that the calibration itself was in error. It was done in the chamber at Bern which, at the time, was apparently experiencing difficulties with low energy ions. There was no independent beam monitor, nor was the measurement checked for repeatability.

In the case of the second order (ray tracing) analysis, it is difficult to argue that the effort should not be pursued. However, it is our opinion, that without supporting calibration data the final results of the effort would be subject to the same objections as the previously described model. The exercise would be intellectually interesting but there would be no way of verifying the final conclusions.

The final recourse is to study the flight data. Comparison of the alignment of the peaks of (presumed) trapped distributions with the 90 deg pitch angle crossings in the Ram Angle Curves suggests a displacement of about 10 deg between MD and ED2 (J. L. Horwitz, private communications).

Examination of the Ram Angle Curves in regions of the plasmasphere where the instrument is switching between ED1 and ED2, shows evidence of a separation in pointing between the two detectors. Since the shape of the curves is proportional to M sin θs, it may be possible to derive a reliable $\Delta\theta$ between the two detectors; although sheath effects could influence this and the picture is complicated somewhat if the two detectors do not have the same β angle width.

For the present we assume that ED1 and ED2 are colinear and are displaced from MD by 10 deg. When the sheath influence on the Ram Angle Curves is better understood [1], and routine curve fits are possible [2], it should be possible to look at the switching data in the plasmasphere as a final verification. (Hugh Comfort's analysis of the ISEE data is summarized in his thin sheath paper [2]. The influences of external effects [i.e., sheath/charging] apparently were never fully determined.)

II. INTER-SENSOR GAINS

Figure 7 shows the approach used for comparing the gain between the various detectors on each head. If the spacecraft is in a predominantly H^+ plasma, and if it is switching gain, and if the mass analyzer is set to H^+, then it would be possible to observe a consistent set of factors between the detectors which would allow all the sensors to be related to one another. In going from ED LO to MD HI, the same total gain should be observed no matter which way we go around the loop. The numbers shown in the figure are approximately the numbers derived from the preflight measurements and calibrations.

NOTE: On the RAM angle plots all measurements have been corrected according to the particular detector on which they were taken and are all adjusted to the most sensitive detector, MD-HI.

To verify these preflight numbers on flight data, regions in the data were located where the instrument was changing ranges (generally near the plasmapause) and the plot program was run with gain factors of unity input. Figures 8a and 8b are examples of the results. (The RAM angle is off in Figure 8a.)

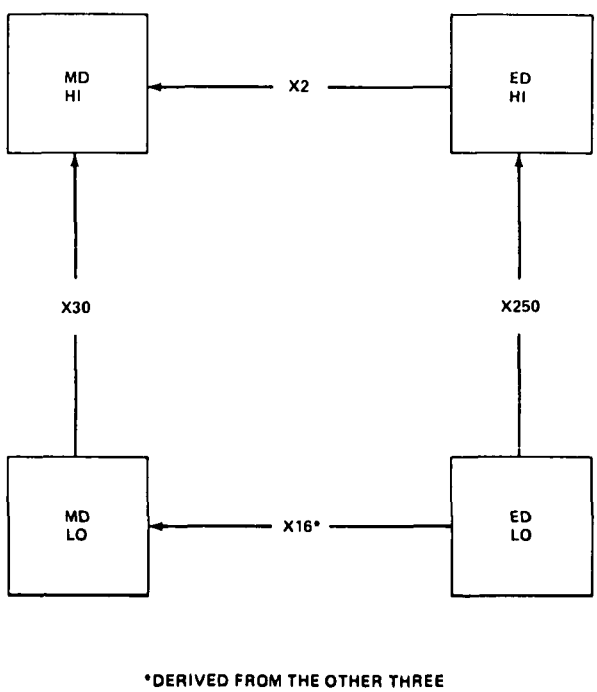

Figure 7. Summary of relative detector efficiencies for Head B, based on pre-flight calibration data.

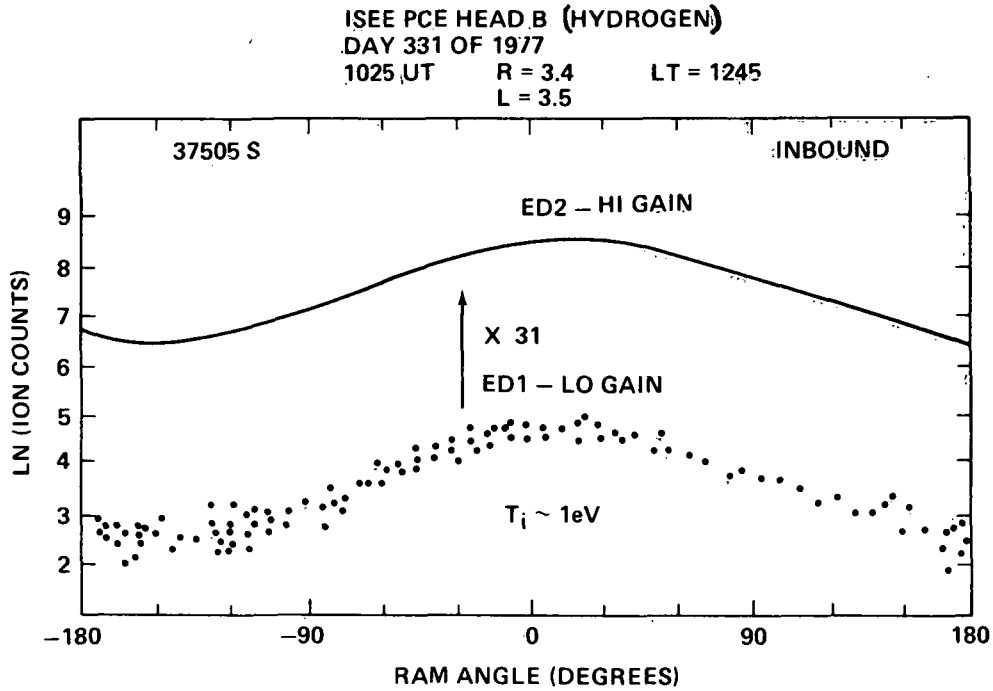

Figure 8a. Flight data from Head B, comparing data from energy detectors 1 and 2.

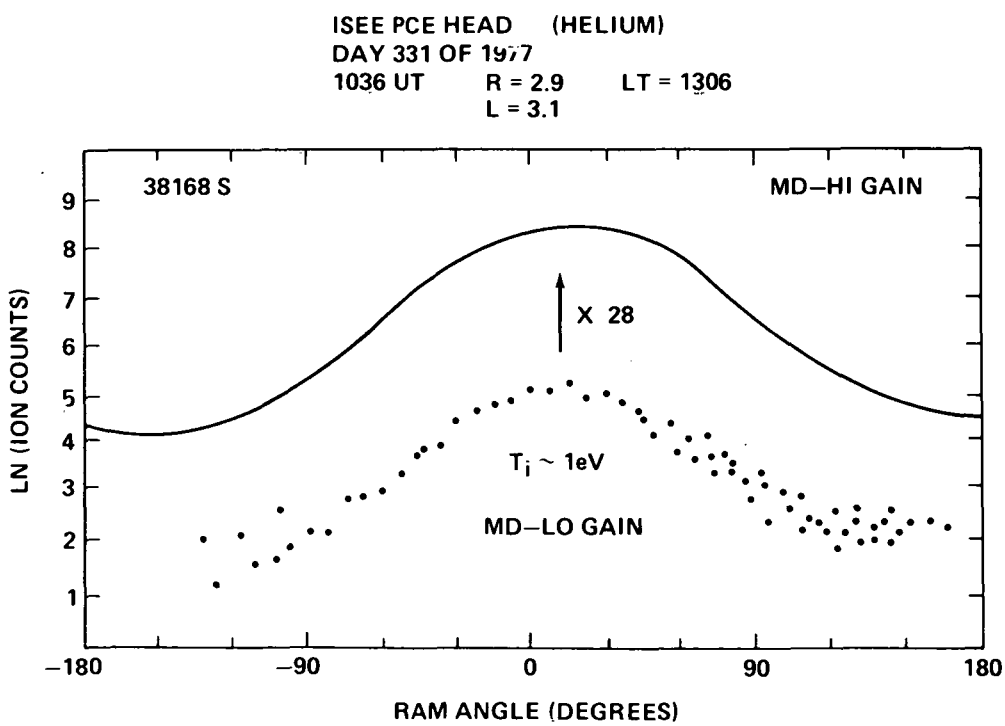

Figure 8b. Flight data from Head B, comparing data from the mass detector at low gain and high gain.

The data taken at the two different settings at zero RPA potential can be clearly seen in the plots. The plot labeled H^+ is the ED detector and the plot labeled HE^+ is the MD detector set on helium. In the two cases a gain of 31.4 is measured between ED-HI and ED-LO and 28.2 between MD-HI and MD-LO. A number of passes were done and the results are listed in Table 1. (NOTE: There was not a great deal of care taken in removing background counts from the data so some of the particularly low measurements may be influenced by it.) (This can be very important in the plasmasphere.)

It is apparent that there is a substantial difficulty in the ED-HI and ED-LO comparison. In view of the results of the previous section, the most likely possibility is that there is a drop in sensitivity in ED-HI. (This was verified at LMSC and Lindau.)

To cross check to the mass analyzer, MD; data from a special calibration called a "bias sequence" was obtained from Day 314, 1977 - outbound. This was a difficult section to analyze because it was taken near the plasmapause and in portions of it there was a fairly high background count. However, it did support a considerably higher ratio between ED-HI and MD-HI, a ratio of the order of 16. Hence, for the first pass through Head B data the gains of Figure 7 were replaced by those shown in Figure 9. (It is noted that they are not self-consistent but neither were the data).

In the latter part of the HEAD B data (the last six weeks), a cold plasma mode was used in which a few spins of H^+ were obtained at about 30-min intervals in MD. A portion of this data has been studied, three samples of which are shown in Figures 10a, 10b, and 10c. These are plots of counts versus RAM angle. The top panel shows the calculated gain factor and markers at the 90-deg pitch angle locations. A factor of 2 seems to be coming out of this set; a number more in agreement with the preflight data, although it is likely that a look at a large amount of data will

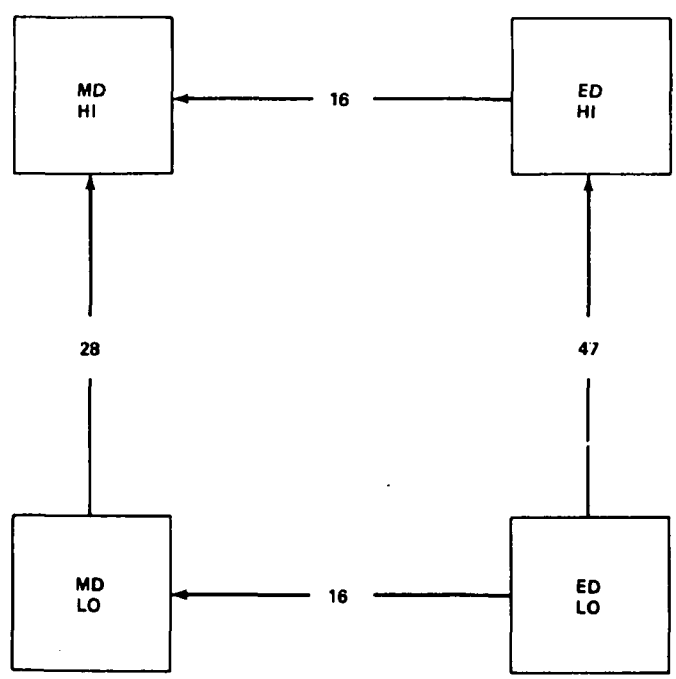

Figure 9. Summary of relative detector efficiencies for Head B, as modified to include results from analysis of flight data, early in the detector life.

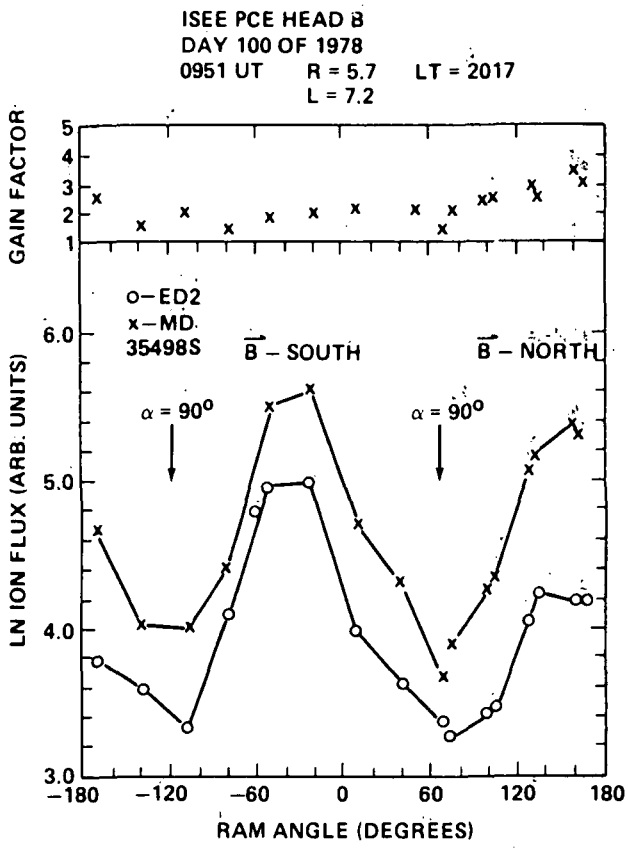

Figure 10a. Pitch angle distributions for H+, showing the ratio of the fluxes for the mass detector and energy detector 2.

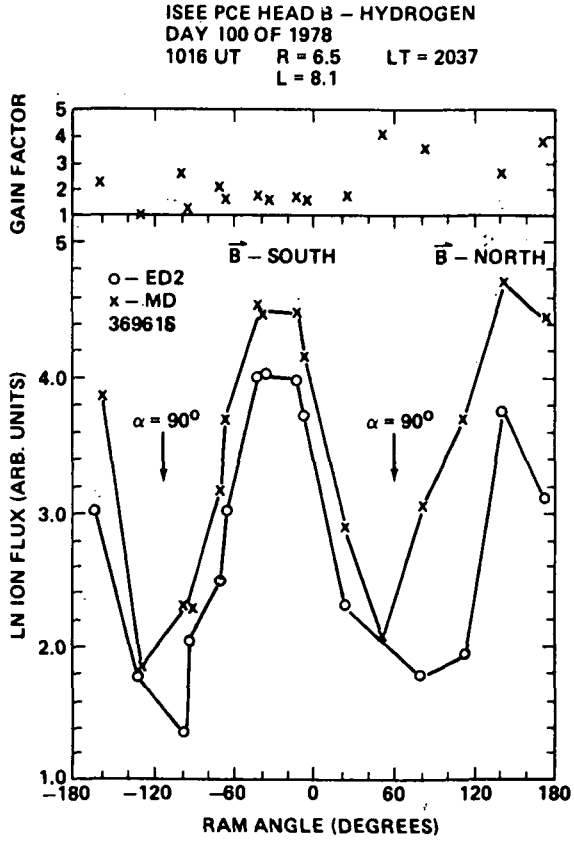

Figure 10b. Pitch angle distributions for Head B, H+, ED2 and MD.

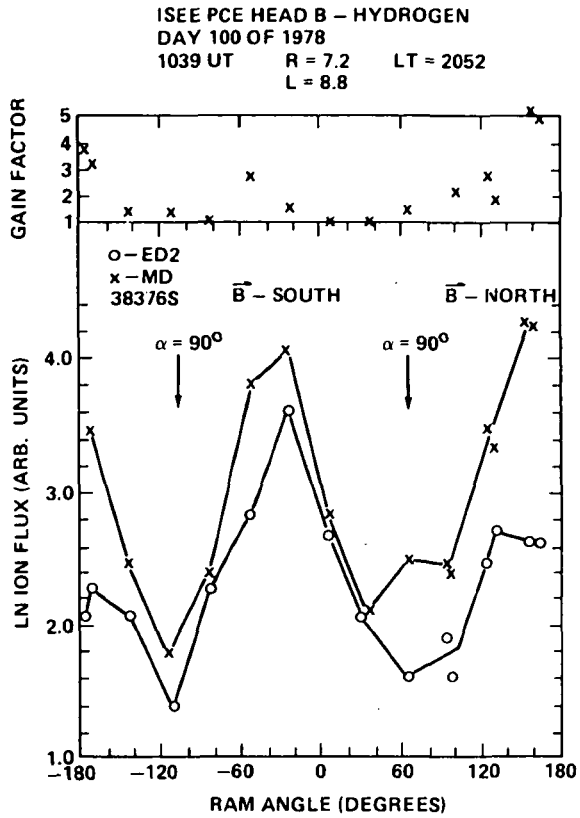

Figure 10c. Pitch angle distributions for Head B, H+, ED2 and MD.

produce results as variable as did the checks between ED-HI and ED-LO. If the results of Figure 10 are to be believed, as well as the results of Table 1, then the gain pattern of Figure 11 would appear to be the proper one.

This, however, brings up one of two very unlikely possibilities:

1) Detectors MD-HI, MD-LO, and ED-HI have all dropped in sensitivity by something close to the same amount.

2) ED-LO has increased in sensitivity by a factor of 4 or so.

There is another possibility. It should be noted that the data of Figure 10 were taken in a region of field aligned flows where the energy of the ambient particles was substantially higher than that of the plasma near the plasmapause of Table 1. Further, at times in the magnetosheath the instrument is observed to auto-range between ED-HI and ED-LO. At these times the gain factor appears to be more like that of Figure 7. It is, therefore, quite possible that the gain factor between ED-HI and ED-LO is energy sensitive by a factor of 6 over the energy range of 0 to 100 V. (E. Shelley notes that this is quite possible. Also, he expects the MD-LO sensitivity to change (drop) with time more than the others. The change will be mass and energy dependent since it is related to the secondary electron production ratio of the incident ions.)

Tentative conclusions regarding ED-2, Head B, are:

1) Its acceptance angle is unknown.

TABLE 1. GAIN COMPARISONS HEAD B

	DAY OF YEAR	ED GAIN RATIO	MD GAIN RATIO
1977	314	16.4	22.7
	321	43.3	31.4
	331	31.4	28.2
	333	43.3	31.4
	341	48.3	31.4
	343	48.3	38.9
	345	48.3	16.4
	352	43.0	43.0
	357	41.0	18.3
	355	43.0	43.0
	360	41.0	22.7
	364	48.3	34.9
1978	002	34.9	----
	009	14.8	31.4
	016	10.7	31.4
	019	66.7	10.7
	021	78.4	13.3
	028	48.3	31.5
	031	10.1	10.1
	033	29.7	34.9
	040	74.2	15.6
	042	48.3	17.4
	054	74.3	43.3
	059	53.8	7.0
	062	10.7	31.4
	064	14.8	22.7
	066	12.6	6.6
	086	----	9.6
	100	25.3	18.3
	MEAN =	39.4	24.9
	STANDARD DEVIATION =	20.0	11.3

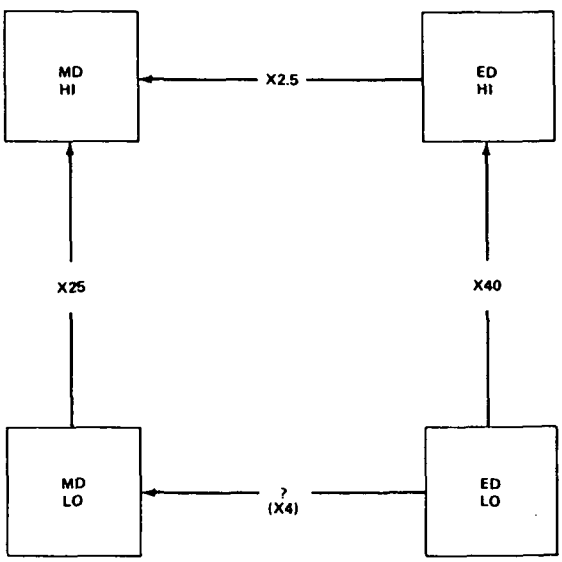

Figure 11. Summary of relative detector efficiencies for Head B, based on flight data, late in detector life.

2) Its pointing direction is uncertain.

3) Its relative sensitivity is variable.

III. DENSITY CALCULATIONS

The counts/second from a limited aperture RPA set to zero volts retarding potential is given by (planar approximation)

$$\text{counts/second} = \frac{A\ \tau\ N}{(\pi)^{3/2} a^3} \int_{\pi + \phi_D - \frac{\alpha}{2}}^{\pi + \phi_D + \frac{\alpha}{2}} \int_{\pi - \theta_o - \frac{\beta}{2}}^{\pi - \theta_o + \frac{\beta}{2}} g(\theta, \phi)$$

$$\times \int_o^\infty v^3 \exp\left(\frac{-[V^2 + V_s^{\ 2} + 2V_s V f(\theta,\phi)]}{a^2}\right) dV d\theta d\phi$$

if the ambient medium is a Maxwellian distribution, and

A = areas of the detector

τ = transmission of the grids

N = ambient density

V_s = spacecraft velocity

a = mean thermal velocity

$g(\theta,\phi) = \sin\theta_o \cos\phi_o \cos\phi \sin^2\theta + \sin\theta_o \sin\phi_o \sin\phi \sin^2\theta + \cos\theta_o \cos\theta \sin\theta$

$f(\theta,\phi) = \sin\theta_s \sin\theta \cos\phi + \cos\theta_s \cos\theta$

and the several angles are defined in Figure 3.

This integral has the pleasant property that its value is relatively constant over a wide range of Mach numbers ($M = V_s/a$).

Therefore, if the above equation is written

$$\text{counts/second} = \frac{A\ \tau\ N}{2} V_s \ \{INT\}$$

where considerable rearranging has been done, it is possible to evaluate the quantity {INT} at some appropriate point and then use this expression over a considerable range at temperatures and flow velocities with little error. The point chosen gave a value of

$$\{INT\} = 0.50$$

and the error resulting from this approximation is shown in Figure 12 for a range of V, T parameter space.

Another pleasant occurrence is that within the plasmasphere the only perturbation to the flow velocity of the plasma is from co-rotation flow, or something close to it, and this tends to be small with respect to the spacecraft velocity and also tends to be at right angles to it. Hence, the co-rotation velocity tends to shift the incoming angle of the flow but contribute little to the resultant speed. Therefore, it is also a fairly good approximation within the plasmasphere to assume the plasma to be flowing at the spacecraft velocity.

Given these two approximations, which together contribute probably less than 20 percent error, it is possible to explore the absolute sensitivity of the ISEE instrument with the expression

$$N = \frac{4 \text{ (counts/sec)}}{(A\tau)\ V_s} \quad .$$

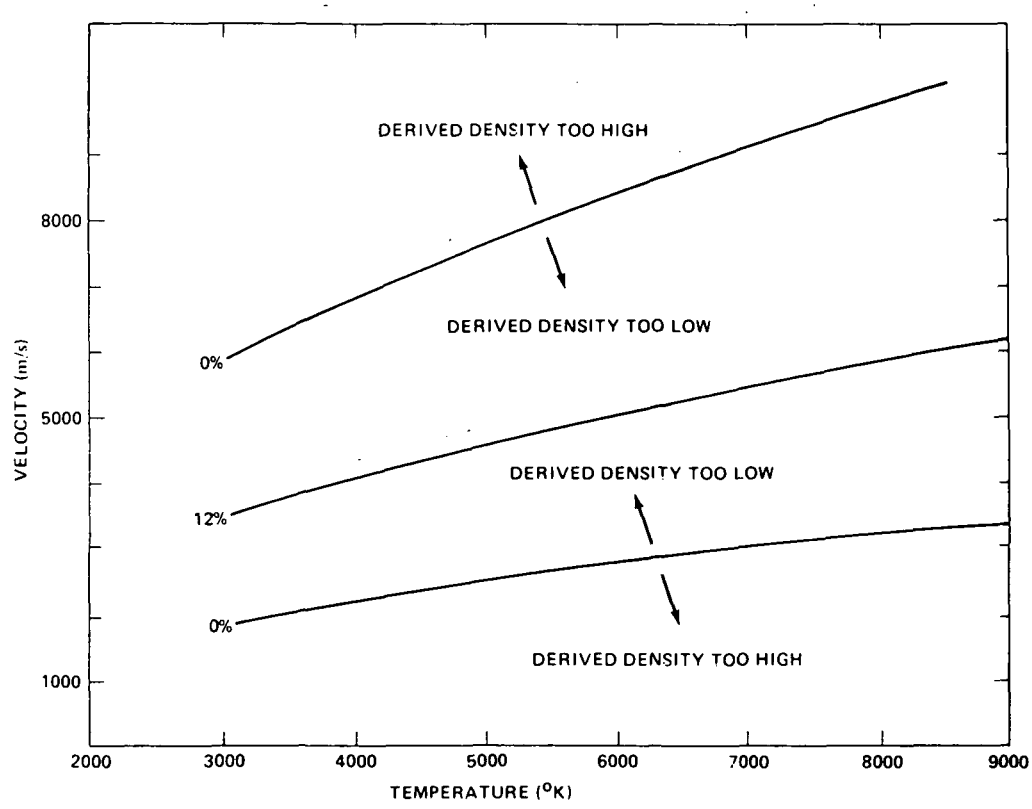

Figure 12. Effects of velocity and temperature on the density calculation.

If N can be determined from an independent measurement, the quantity, $A_{eff} = (A\tau)$ can be derived from the data and compared with preflight measurements. This was done for time points in the early data using the upper hybrid resonance measurements and the results are listed in Table 2. All measurements are for ED1, Head B.

TABLE 2. EFFECTIVE AREA CALIBRATION

1977 DOY	TIME (UT)	COUNTS PER SEC.	DENSITY (IONS/CM^3)	VS. (M/SEC)	A_{eff} (mm^2)
329	?	29665	1985	6931	8.62×10^{-3}
333	19:53	14710	1117	6015	8.76×10^{-3}
336	5:28	14719	1117	6861	7.68×10^{-3}
350	13:36	17994	1117	6861	9.39×10^{-3}
362	12:25	16291	1117	7013	8.32×10^{-3}
				A_{eff} =	8.55×10^{-3}

The preflight information was as follows:

$$A_{eff} = (\text{physical area of detector}) \times (\text{grid transmission})^{(\text{number of grids})}$$

$$\times\ (\text{channeltron efficiency})$$

$$= (30 \times 10^{-3}\ \text{mm}^2)\ (0.9)^3\ (0.33)$$

$$= 7.22 \times 10^{-3}\ \text{mm}^2 \quad .$$

A close comparison!

Alternatively, this approach can be used to estimate density directly from the RAM angle plots if the plasma meets the criteria of corotating, thermal, and Maxwellian. The numbers on the plots are actually counts per frame but have been adjusted for the relative gain between the detectors such that they appear to be coming from MD2. This leads to the equation for density of

$$N = \left(\frac{\text{counts}}{\Delta t}\right) \frac{2}{(A_{eff})\ (G_1)\ (G_2)\ \{INT\}\ V_s}$$

where

Δt is the time interval of the frame accumulation (0.219 sec)

G_1 is the gain factor between ED2 and MD2 (G_1 = 16 in most of the plots)

G_2 is the gain factor between ED1 and ED2 (G_2 = 47 for most of the plots).

$\{INT\} = 0.50$

$N = (3.36)\ \underline{\text{counts}}$

where V_s is in meters/sec, N is in ions/cm^3, and counts are from the plots.

This approach was used to determine the density in the plasmasphere for several passes and the results were compared with the wave data by Hugh Comfort. An example of the results is shown in Figure 13.

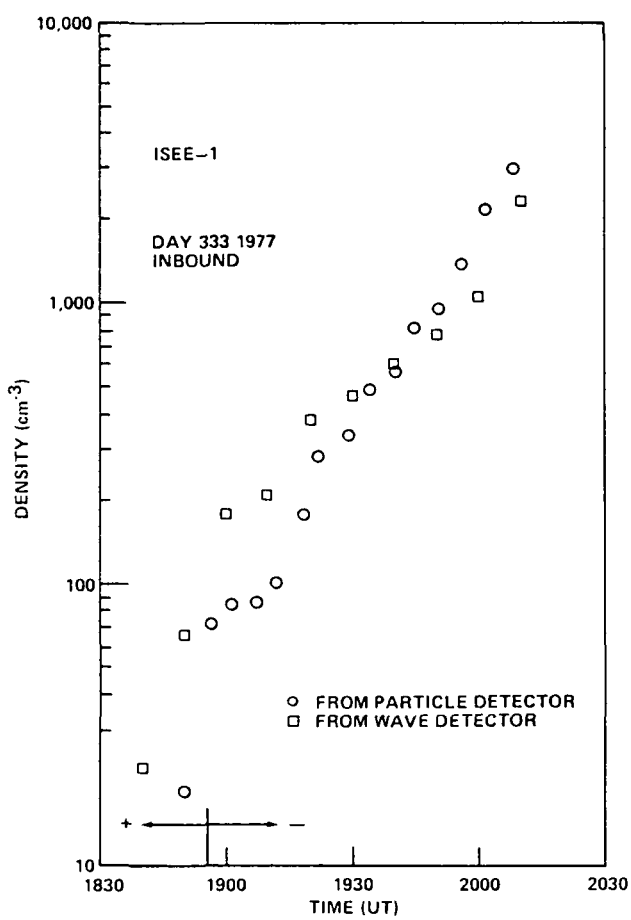

Figure 13. Comparison of plasmasphere density profiles obtained from the PCE and the plasma wave instrument.

This particular pass is admittedly one of the better comparisons, however, they all at least were "in the ball park." In general, the results showed that the Plasma Composition Experiment was overestimating the density by about a factor of two when ambient densities were in the 1500 to 2000 ions/cm^3 range and underestimating the density by a factor of perhaps 4 or 5 when the ambient density was in the 100 ion/cm^3 range. The error is at least in the right direction to be explained by spacecraft potential. At present the best guess is that the spacecraft is of the order of 0.5 V negative at the higher density range at 1000 to 2000 ions/cm^3, increases to the neutral point at about 100 to 50 ions/cm^3 and goes positive at smaller densities. This question will presumably be answered if Mozer's data is ever figured out.

Singh has looked at the enhancement of current to a limited aperture RPA when the spacecraft is negative. Table 3 lists some preliminary results for a 45 x 45 deg aperture. They are given for comparison purposes.

TABLE 3. SATELLITE POTENTIAL EFFECTS ON CURRENT TO AN RPA

$q\phi_s/kT$	-1	-2	-3	-4	-5	-10
Enhancement	2	3	3.9	4.7	5.5	8.3

Of course, from physical considerations it would be expected that the crossover in density determinations would occur at the point where the spacecraft goes through zero potential. If there were to be forced on the data, it would tend to lower the effective area of ED1 by about a factor of four and would indicate enhancements in the density measurements by as much as a factor of 10 in the vicinity of 2000 ions/cm^3.

Finally, Table 4 is from a note obtained from W. K. Peterson. These numbers give his last guess for geometric factors for MD and ED for Head A and Head B for several mass species in the low energy channel of the instrument. These were apparently derived from a combination of calibration fits to analytic instrument models and were influenced by flight data. They are for the low gain detectors. The analysis assumes the energy passband is filled. The ratio of $G\delta E$ for MD and ED should be observed in the data if the environment is all H^+ and MD is set on 57. These data are the result of best fits for 5 or 6 magnetosheath intervals in October and November of 1977, counts/second = $G\delta E$ flux/keV.

TABLE 4. GEOMETRIC FACTORS

For ESTEP = 0

ED		HEAD A	HEAD B
	$G\delta E$	Ec = 49 eV 0.19×10^{-3}	Ec = 54 eV 0.20×10^{-3}
MD		Ec = 40 eV	Ec = 44 eV
H^+	$G\delta E$	0.36×10^{-3}	0.37×10^{-3}
He^{++}	$G\delta E$	0.45×10^{-3}	0.53×10^{-3}
He^+	$G\delta E$	0.72×10^{-3}	0.56×10^{-3}
O^+	$G\delta E$	0.31×10^{-3}	0.52×10^{-3}

IV. ENERGY PASSBAND-BIAS CHECKS

There is an influence of the instrument on the energy distribution of incoming particles in the lowest channel of the electrostatic analyzer. This channel, nominally 100 eV in width but more likely about 150 eV in width, has a response versus energy which is Gaussian. Although the influences of this characteristic are probably only important for high temperature, low Mach number plasma, it should be noted. The only measurements of this response were done in flight during the "bias sequences" mentioned previously. These measurements were done within the plasmasphere in the presence of a cold plasma and the bias on the electrostatic analyzer was moved in 25-V steps to sweep the passband across the incoming cold beam. The measurements from DOY 314, 1977, have been analyzed.

Figure 14 is an example of the results of one such sequence (J. L. Horwitz, private communication). This one is for MD Low Gain, Head B. The x-axis is steps (approximately 25 V), the y-axis is counts.

The other possible area of influence of the energy distribution is from sheath effects. These are currently under study by Singh and would be expected to be small at the higher energies but could be important at the lower energies of the plasmasphere, particularly in the area of determining the spacecraft potential from the ion data.

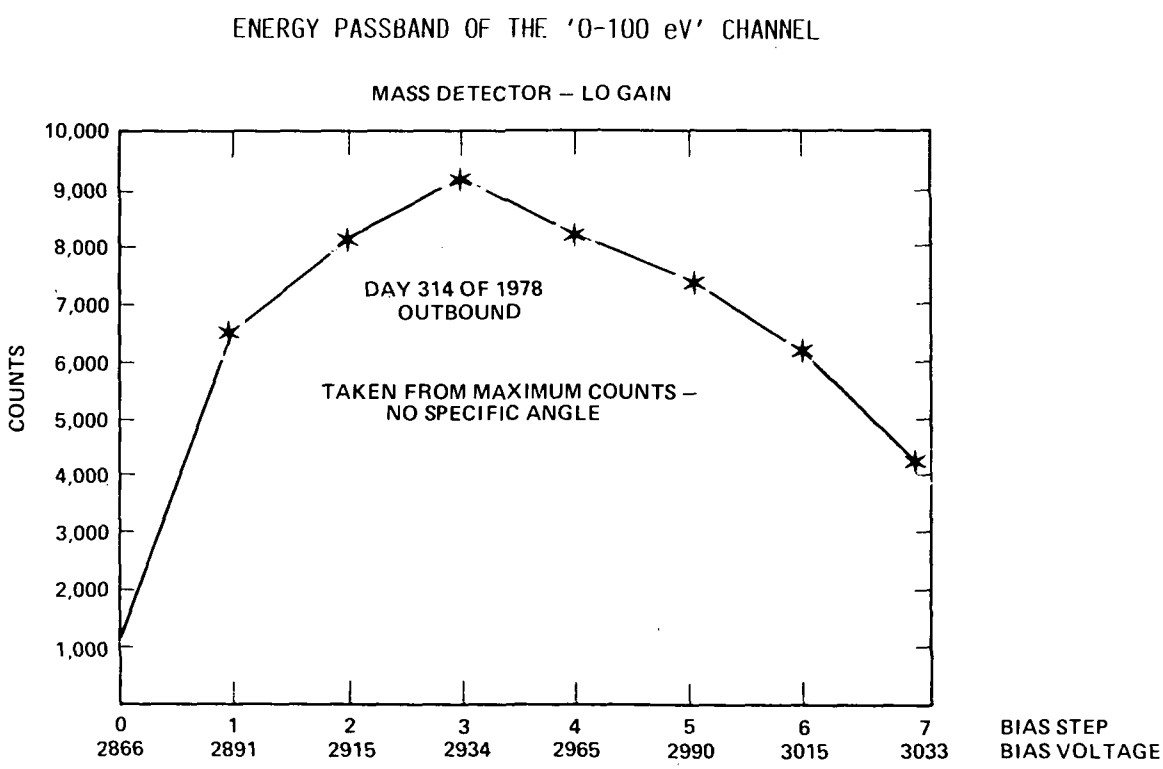

Figure 14. Characteristics of the electrostatic analyzer response in the RPA mode, Head B, flight data.

V. HEAD A CALIBRATION

(Predicted Energy Response of the Sharp ISEE Instrument at the Lowest Energy Step)

Figures 15 and 16 show the predicted ED2 and MD energy response at E-STEP 00000 for sensors A and B, respectively. The vertical scale is counts normalized to 1; the horizontal scale, energy in eV, is in units of 20 eV per major division. Rather than fix the external energy scale and draw eight response curves, one for each B-STEP, one response curve requiring that the energy scale be shifted appropriately for each B-STEP has been drawn. The eight points indicated on the abscissa are the zero points corresponding to the eight subscripted B-STEPs. Thus, for sensor A, the ED2 energy response centerline is +13 eV at B-STEP 110, -4 eV at B-STEP 111, etc. The ED2 and mass analyzer (MA) energy response curve shapes are scaled from measured data taken with an $_2H^+$ beam at E-STEP 00001 and B-STEP 011 (sensor B) or B-STEP 101 or 100 (sensor A).

The scaling was based on the following equations:

$$E_{in} = E_X + V_c = \text{constant at any given E-STEP} \tag{1}$$

$$E_{0X} = E_{1X}\left(\frac{\Delta V_0}{\Delta V_1}\right) - V_c\left(1 - \frac{\Delta V_0}{\Delta V_1}\right) \tag{2}$$

$$V_c = V(R_c) = \Delta V\left[\frac{\ln(R_c/R_{inner})}{\ln(R_{outer}/R_{inner})}\right] - V_{inner} - \Delta B \tag{3}$$

$$K_i = \frac{E_{in\ c\ i}}{\Delta V_i} = \frac{E_{x\ c\ i} + V_{c\ i}}{\Delta V_i} \tag{4}$$

where

E = particle energy

V = voltage or energy depending on context

ΔV = potential difference between ESA deflection plates

ΔB = voltage or energy difference between B-STEP settings

R = radius of ESA plates or center trajectory

K = analyzer constant

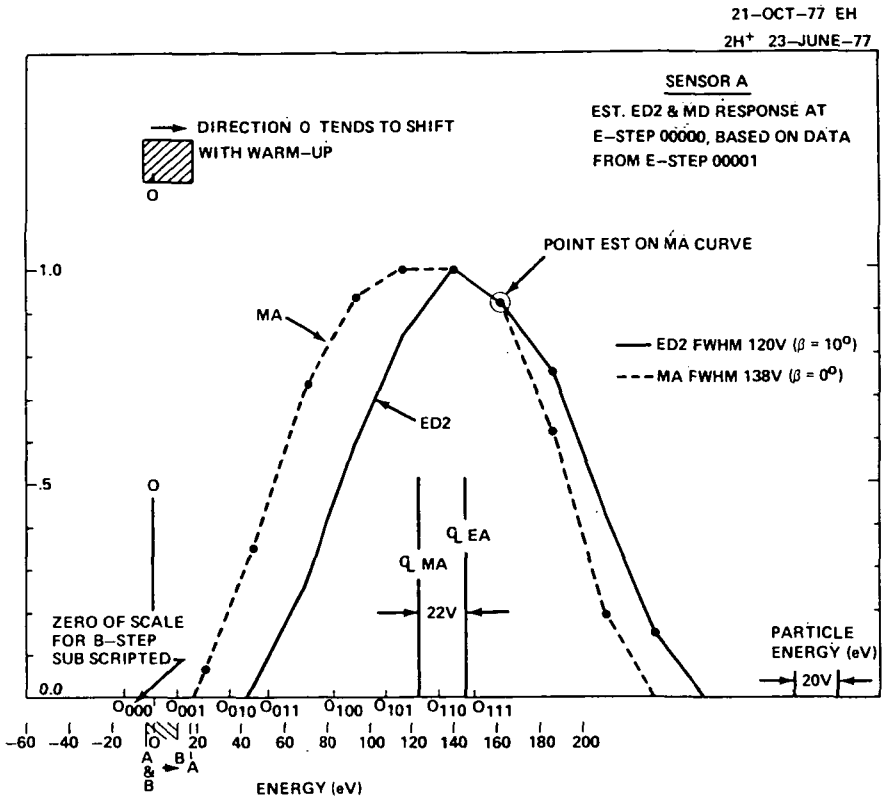

Figure 15. Characteristics of the electrostatic analyzer response in the RPA mode, Head A, ED2 and MD, laboratory.

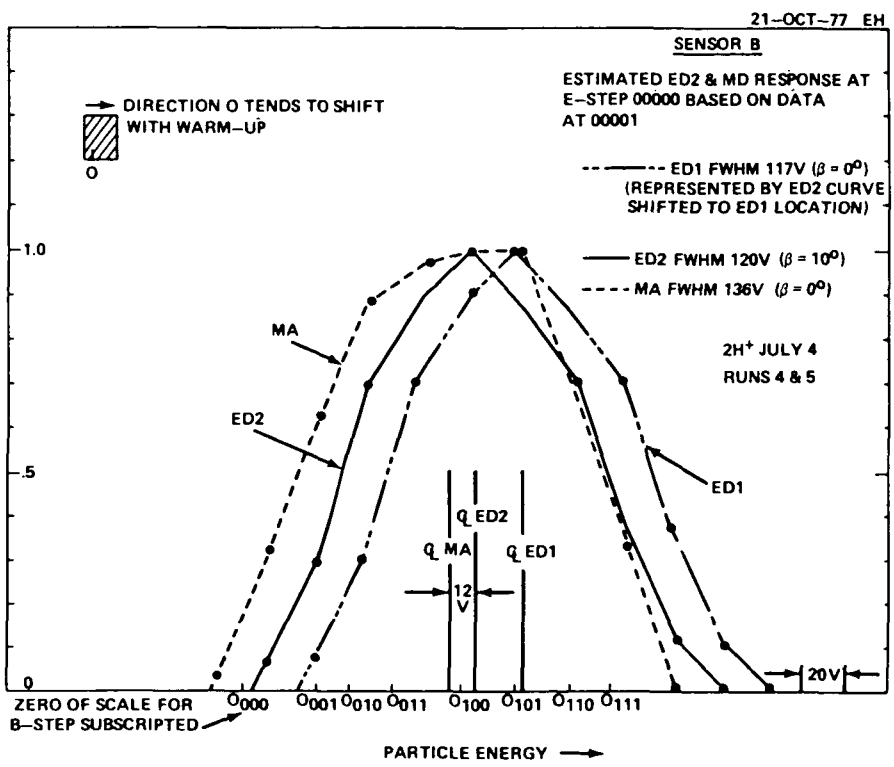

Figure 16. Characteristics of the electrostatic analyzer response in the RPA mode, Head B, ED2 and MD, laboratory.

and subscripts

in = internal

X = external

c = center

i = E-STEP index

0 = E-STEP 00000

1 = E-STEP 00001

inner = inner ESA plate

outer = outer ESA plate.

Particles entering on a centerline trajectory are assumed to be preaccelerated to the center potential in the ESA, V_c. Inner and outer ESA plate voltages and ΔB's were measured in atmosphere at 10°C prior to calibration in vacuum. These were used to calculate ΔV_i and V_c. E_{1X} was taken to be the center of the full width at half maximum (FWHM) of the EA energy data measured in vacuum. Energy values for those data were read from a digital voltmeter indicating source potential of the ${}_2H^+$ beam. Initially the analyzer constant K of each EA and MA was assumed constant for all i. This allowed E_{0X} to be calculated from E_{1X} at the B-STEP at which E_{1X} was measured by applying equation (2). $FWHM_0 = (E_{0in}/E_{1in})\ FWHM_1$, approximately 6.5 percent narrower. Finally, the zero positions on the scale for all B-STEPS are determined by adding or subtracting the appropriate ΔB.

It was discovered during calibration in vacuum with a particle beam, however, that the high-voltage power supplies were not quite sufficiently temperature compensated, and thus during operational warmup ΔV_i diminishes. This problem was treated using equation (4) as though ΔV_i were constant and K_i variable. The percent variation in K_i is a measure of percent variation in ΔV_i. K_i versus E and E-STEP is plotted for sensor A, EA and MA in Figures 17 and 18, respectively, and for sensor B in Figures 19 and 20, respectively. The range of variation at the E-STEP 00000 position was assumed equal to the 00001 data range plus 25 percent margin on either side for sensor A and 50 percent margin on either side for sensor B. This range of uncertainty is reflected in Figures 15 and 16 by the sketches in the upper left-hand corner depicting a band of uncertainty around any given zero point. The arrow indicates the direction in which the zero tends to shift as the instrument warms up. For sensor A, the uncertainty band is explained thus.

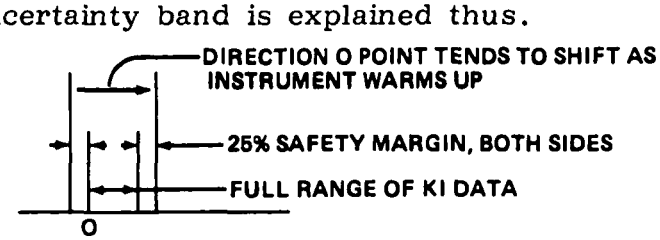

For the initial turn-on, B-STEPs 101 for sensor A and 011 for sensor B are proposed.

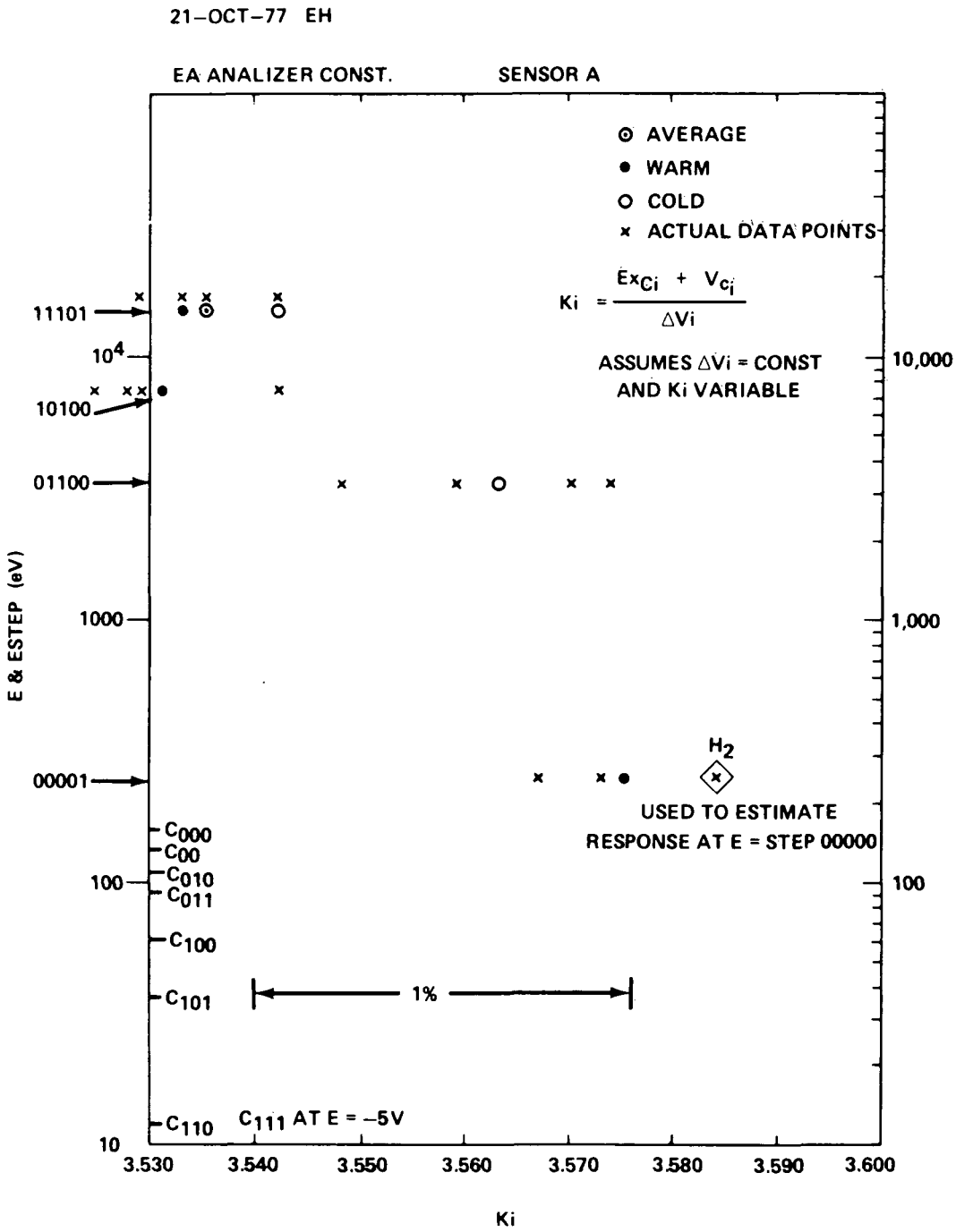

Figure 17. Analyzer constant for Head A, energy detector (ED).

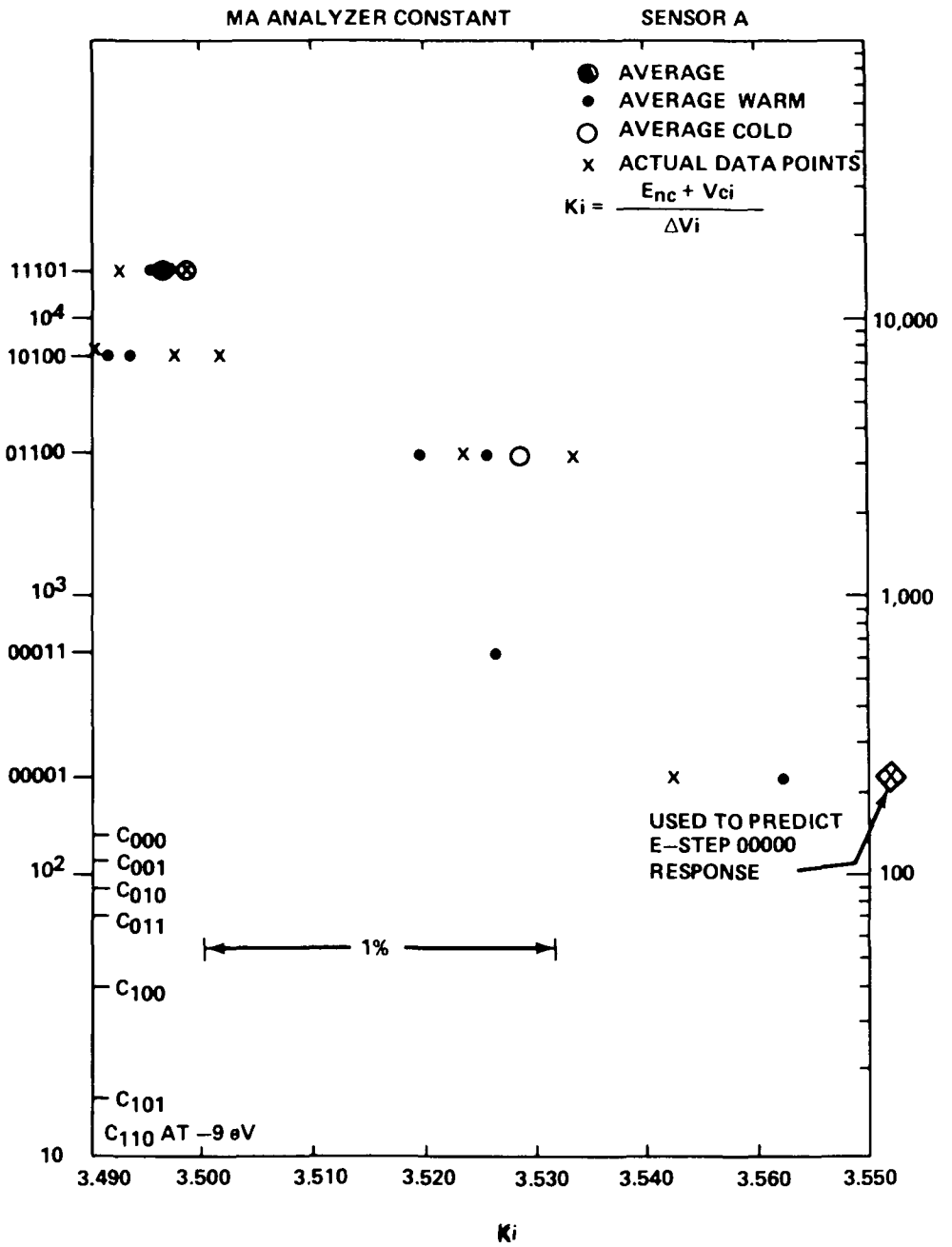

Figure 18. Analyzer constant for Head A, mass detector (MD).

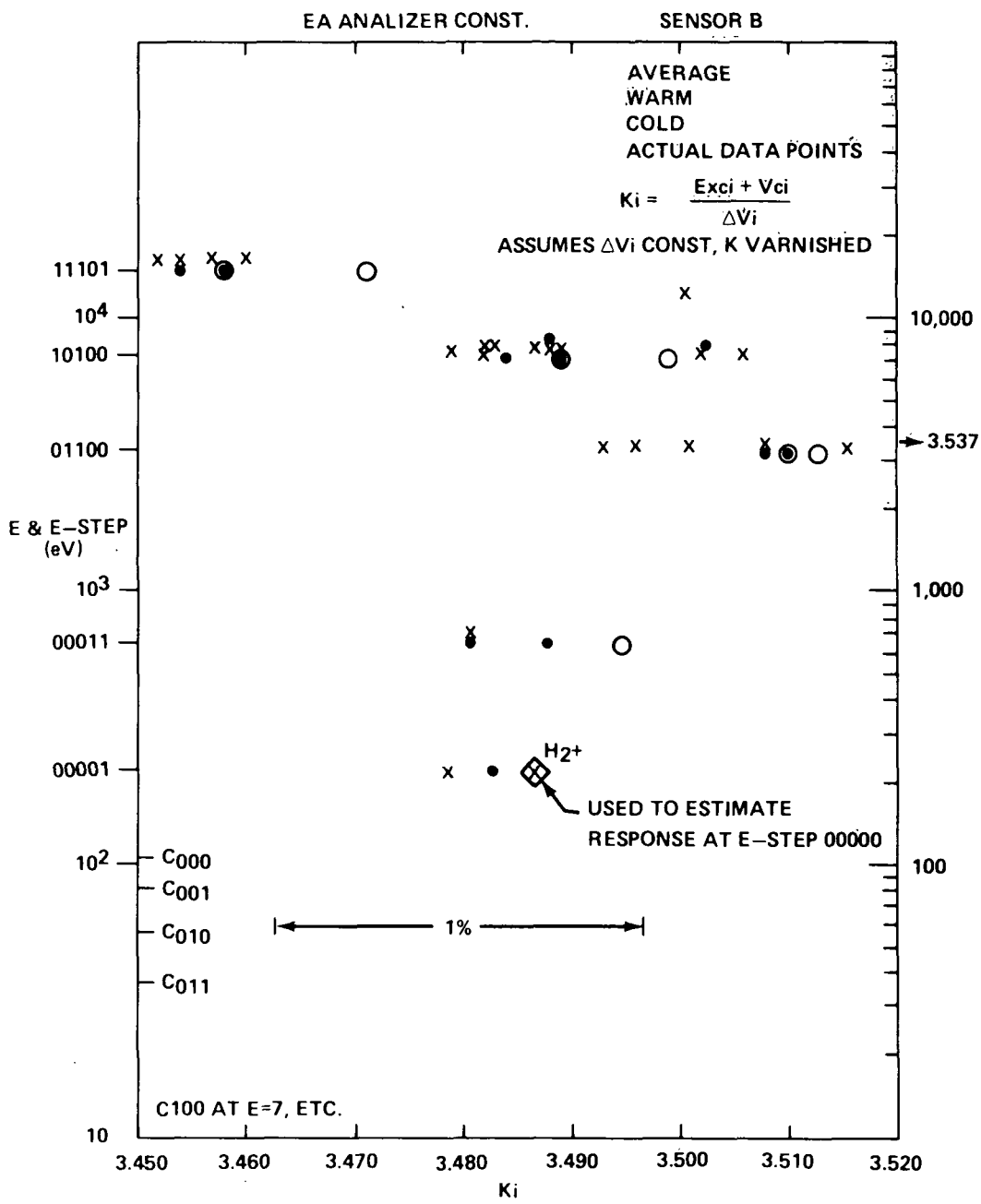

Figure 19. Analyzer constant for Head B, energy detector (ED).

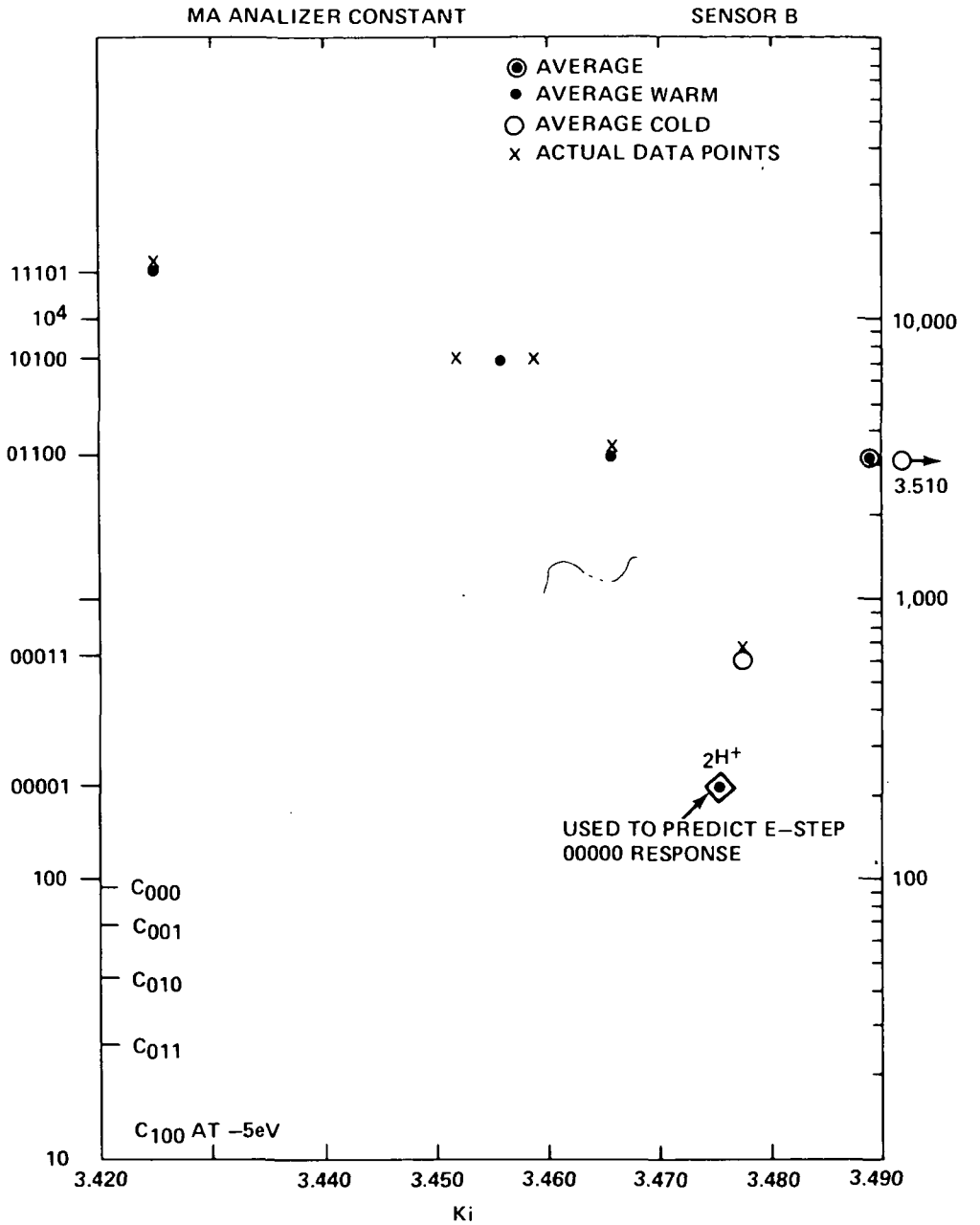

Figure 20. Analyzer constant for Head B, mass detector (MD).

For sensor B, the ED1 energy response was determined by fixing the $_2H$ beam energy at 19 ± 1 eV and measuring count rate as a function of B-STEP. The experimental ED1 data and the predicted ED2 response curve are plotted in Figure 21. They suggest that the ED1 response peak is about 21V higher than that of the ED2. There are no other calibration data against which to check this result. The ED1 response is represented on Figure 16 by scaling the ED2 response curve to the correct width and location.

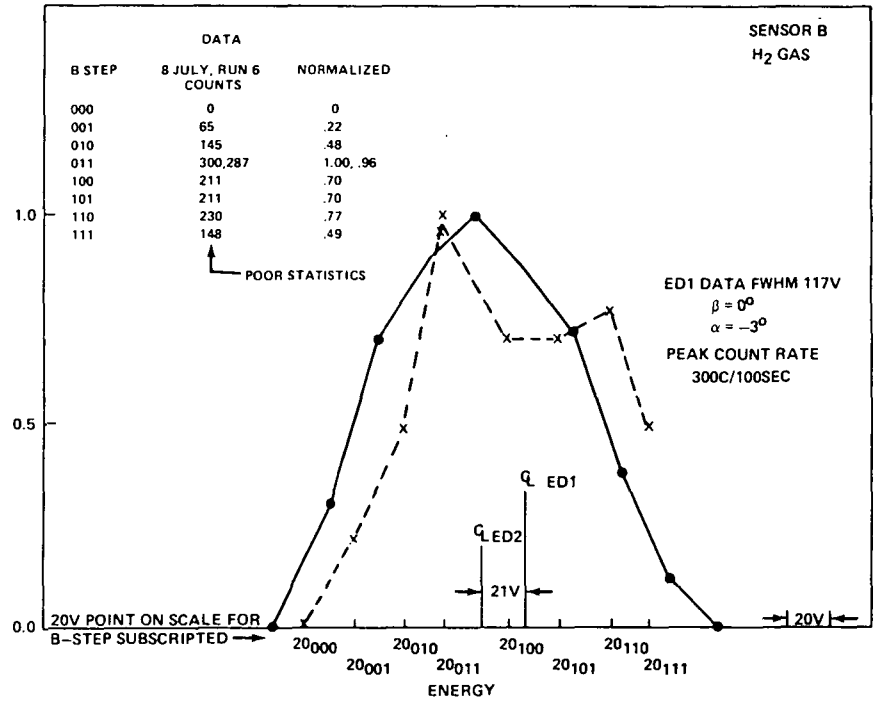

Figure 21. Characteristics of the electrostatic analyzer response in the RPA mode, Head B, ED1, laboratory.

VI. RAY TRACING

The ray tracing analysis for the PCE is as follows:

1) Refer to Figures 22, 23, and 24 for diagrams and dimensions.

2) θ_1 is measured in the x-z plane and θ_2 is measured in y-z plane.

3) Assume that $E = E_z$, $E_x = E_y = 0$ between B2 and G, between G and B3, and between B3 and S1. Assume E = 0 between the entrance aperture and B2, between S1 and the analyzer entrance, and between the analyzer exit and S2.

4) Assume that the Fringing Field correction at the analyzer entrance and exit can be made by a refraction approximation.

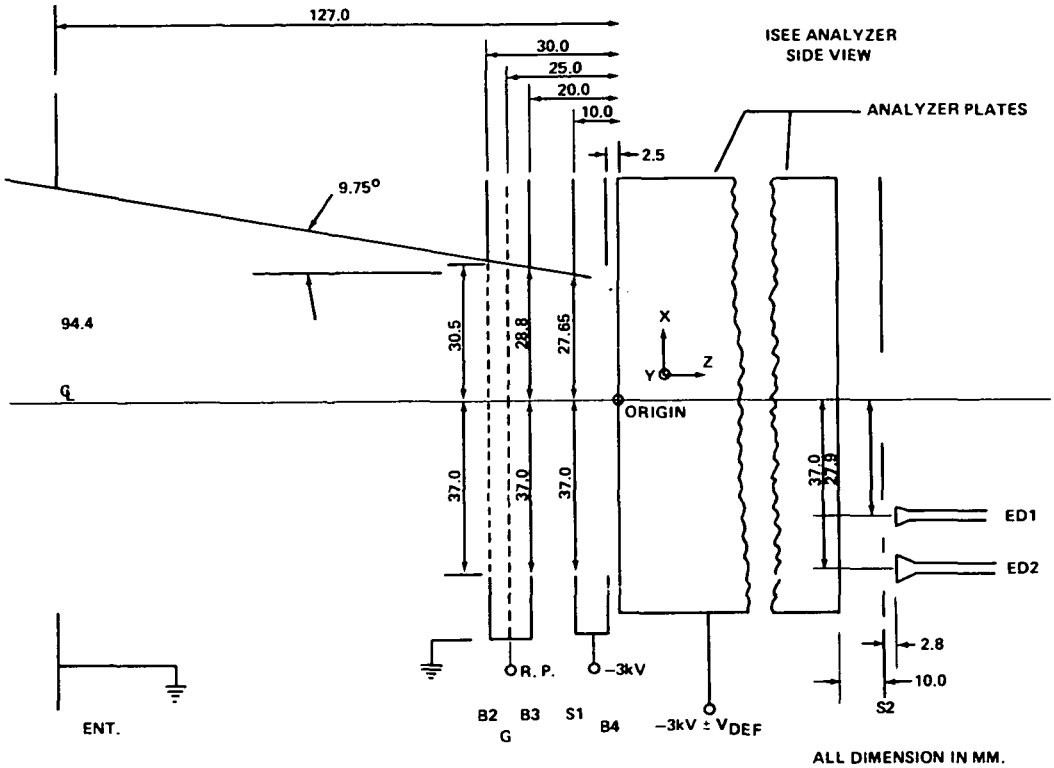

Figure 22. PCE optical path, ray tracing version.

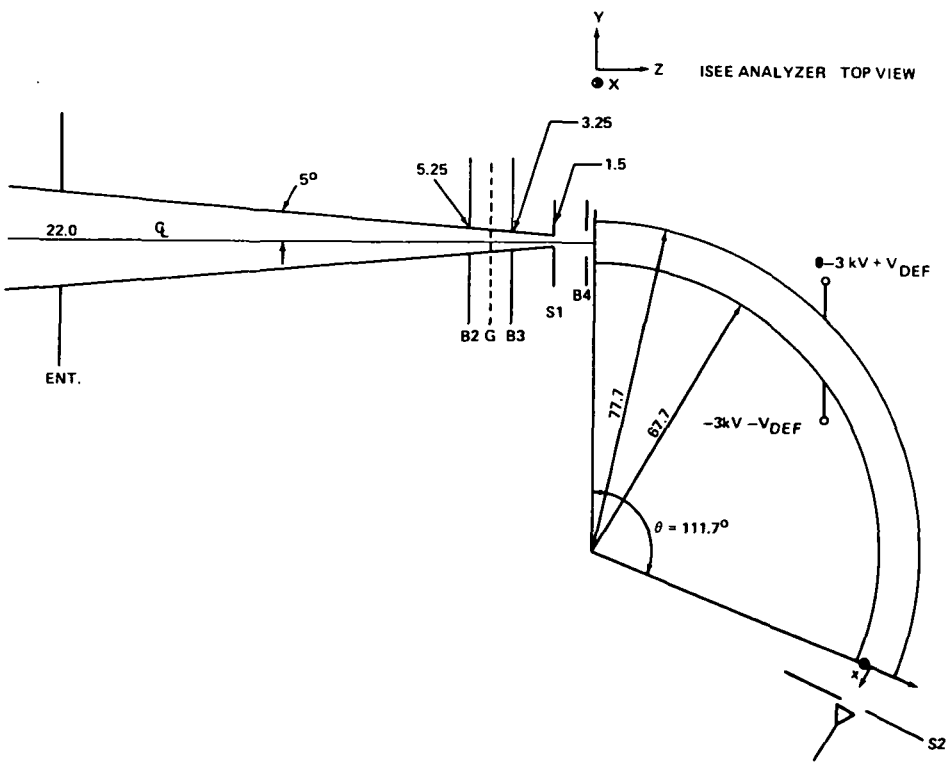

Figure 23. Electrostatic analyzer plates.

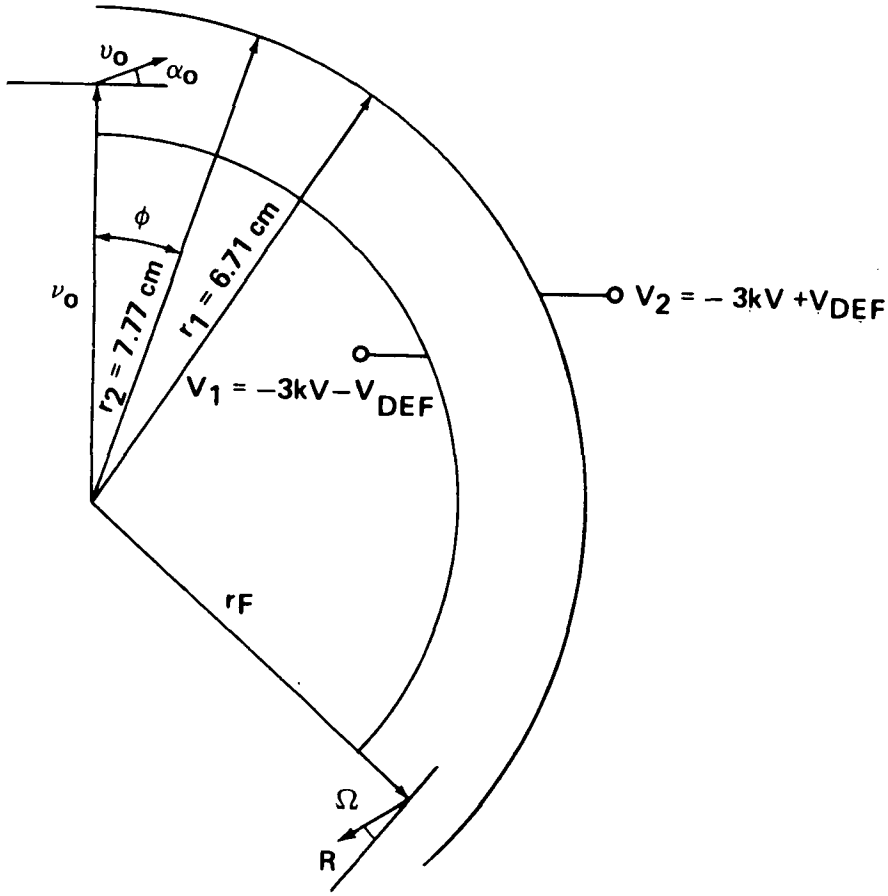

Figure 24. Details of electrostatic analyzer plates.

Detailed Procedure

1) Let x_1, y_1, be coordinates in the plane of the entrance aperture and let x_2, y_2 be coordinates in the plane of grid B2. To select a particle, choose at random x_1, y_1, x_2, y_2 subject to the restrictions $-4.72 \leq x_1 \leq 4.72$; $-1.1 \leq y_1 \leq 1.1$; $-3.7 \leq x_2 \leq 3.05$; and $-0.263 \leq y_2 \leq 0.263$.

2) Let θ_1 be the angle of the particle direction in the x-z plane and θ_2 be the angle of the particle direction in the y-z plane. From the geometry:

$$\theta_1 = \tan^{-1}\left(\frac{x_1 - x_2}{9.7}\right)$$

$$\theta_2 = \tan^{-1}\left(\frac{y_1 - y_2}{9.7}\right)$$

$$-40.9° \leq \theta_1 \leq 38.7°$$

$$-8° \leq \theta_2 \leq 8° \quad .$$

3) Set up 3 matrices with coordinates θ_1, θ_2 in 1° x 1° increments. M_o will record the "unsuccessful" particles, M_1 will record the "successful" particles that strike ED1 and M_2 will record the "successful" particles that strike ED2.

4) To start the computation, find the initial location and velocity components of grid B2. These are:

$$z_o = -3.0$$

$$x_o = x_2$$

$$y_o = y_2 \quad .$$

Define $D = [9.7^2 + (x_1 - x_2)^2 + (y_1 - y_2)^2]^{\frac{1}{2}}$. (D is the total distance traveled between the entrance aperture and B2).

$$V_o = \text{initial particle velocity} = \left(\frac{2\varepsilon_o}{m}\right)^{\frac{1}{2}}$$

$$v_{xo} = \frac{V_o\,(x_2 - x_1)}{D} = -V_o \sin\theta_1$$

$$v_{yo} = \frac{V_o\,(y_2 - y_1)}{D} = -V_o \sin\theta_2$$

$$v_{\zeta o} = V_o \left(\frac{9.7}{D}\right) \quad .$$

5) Between B2 and G, $E_x = E_y = 0$,

$$E_z = \frac{-V_{RPA}}{\Delta z \times 299.7295} = \frac{-V_{RPA}}{149.86475}$$

The equations of motion are:

a) $x' = x_o + v_{xo}t$

b) $y' = y_o + v_{yo}t$

c) $z' = z_o + v_{zo}t + 1/2$

d) $v_{x'} = vxo$

e) $v_{y'} = vyo$

f) $v_{z'} = vzo^{+}$

$$z' = z(G) = -2.5; \quad z_o = z(B2) = -3.0 \quad .$$

Equation C can be solved for t giving:

$$t = \frac{-V_{zo} \pm \sqrt{V_{zo}^{2} + 2(Z' - Z_o)\frac{e}{m}E_z}}{\frac{eE_z}{m}} \quad .$$

Case A: $b^2 - 4\,ac < 0 \rightarrow$ no real solution for t exists, i.e., the particle is stopped by the retarding potential.

Case B: $b^2 - 4\,ac > 0$ and $[b^2 - 4\,ac]^{\frac{1}{2}} \leq |v_{zo}| \rightarrow$ there will be two positive solutions for t. Pick the smallest positive value.

Case C: $b^2 - 4\,ac >$ and $b^2 - 4\,ac^{\frac{1}{2}} > |v_{zo}| \rightarrow$ there will be one positive and one negative solution for t. Pick the positive solution.

After finding t (assuming a real value exists), use equations (a), (b), and (f) to compute x', y', v_z'.

If $v_{RP} \equiv 0$, then the quadratic solution is undefined. In that case use:

$$t = \frac{Z' - Z_o}{V_{zo}}$$

and then use equations (a), (b), and (f) to compute x', y', v_z'.

6) At grid G, a new computation is started. So redefine the initial positions and velocities according to:

$$\left.\begin{aligned} x_o &= x' \\ y_o &= y' \\ v_{xo} &= v_{x'} \end{aligned}\right\} \quad \text{From results of part 5}$$

$$\left.\begin{array}{l} v_{yo} = v_{y'} \\ v_{zo} = v_{z'} \end{array}\right\} \quad \text{From results of part 5}$$

$$z' = -2.0$$

$$z_o = -2.5$$

$$E_x = E_y = 0; \quad E_z = \frac{V_{RPA}}{\Delta z \times 299.7295} = \frac{V_{RPA}}{149.86475} \quad .$$

Repeat the procedure outlined in (5) above to trace the particle from G to B3. Again, pick the smallest positive real value for t. B3 is a limiting aperture, and so at B3 need to check if $-3.7 < x' < 2.88$ and $-0.1625 < y < 0.1625$. If both these conditions are not met, then the particle was not "successful."

7) At Grid B3, a new computation is started. So redefine the initial positions and velocities according to:

$$\left.\begin{array}{l} x_o = x' \\ y_o = y' \\ v_{xo} = v_{x'} \\ v_{yo} = v_{y'} \\ v_{zo} = v_{z'} \end{array}\right\} \quad \text{From results of part 6}$$

$$z' = -1.0$$

2935 E.G.S. 6/23/76

$$z_o = -2.0$$

$$E_x = E_y = 0; \quad E_z = \frac{3000}{299.7295} = 10.0069 \text{ statvolts/cm} \quad .$$

Trace the particle from B3 to S1 using the procedure outlined in (5) above. Since this is an accelerating potential region, the quadratic solution for t will result in one positive and one negative solution for t. Pick the positive solution. S1 is a limiting aperture, and so at S1 need to check if $-3.7 < x' < 2.765$ and $-0.075 < y' < 0.075$. If these conditions are not met, the particle is not "successful."

8) Between S1 and the analyzer plate entrance, the particle is in a zero-field region. Re-initialize the position and velocity according to:

$$\left.\begin{aligned} x_o &= x' \\ y_o &= y' \\ v_{xo} &= v_x' \\ v_{yo} &= v_y' \\ v_{zo} &= v_z' \end{aligned}\right\} \quad \text{From results of part 7}$$

$$z_o = -1.0$$

$$z' = 0 \quad .$$

The equations of motion are:

a) $x' = x_o + v_{xo}t$

b) $y' = y_o + v_{yo}t$

c) $z' = z_o + v_{zo}t$

d) $v_z' = v_{zo}$

Solve (c) for t and then use (a) and (b) to find x', y'. Also, $v_x' = v_{xo}$, $v_y' = v_{yo}$.

9) <u>Tracing Particle Through the Analyzer Plates</u>

At the entrance to the plates, change from cartesian to cylindrical coordinates (r, ϕ, ζ). The electric field is radial, $E_r = -A/r$, $E\phi = E_\zeta = 0$.

$$E_r = -\frac{1}{r}\left(\frac{v_2 - v_1}{\ln(r_2/r_1)}\right) = \frac{2V\,\mathrm{def}}{r\,\ln(r_2/r_1)} \quad .$$

The potential is:

$$\phi(r) = \frac{V_1 \ln\left(\frac{r_2}{r}\right) + V_2 \ln\left(\frac{r}{r_1}\right)}{\ln\left(\frac{r_2}{r_1}\right)}$$

The potential outside of the plates is $\phi_o = -3kV = -10.0069$ statvolts. The potential inside the plates is $\phi(r)$ which is not in general equal to ϕ_o. Hence, there is a refraction at both the entrance and exit of the plates which causes a change in v_{zo} and hence a change in angle. Let x_o, y_o, $z_o = 0$, v_{xo}, v_{yo}, v_{zo} be the initial coordinates and velocities in the analyzer plate entrance. The effect of refraction is to change v_{zo} to v_{zo}' according to the equation:

$$V_{zo}' = \left[\frac{2e}{m}\,(\phi_o - \phi(r)) + V_{zo}^{\,2}\right]^{\frac{1}{2}}$$

where

$$r = 7.27 + y_o$$

$$\phi_o = -10.0069$$

$$\phi(r) = \frac{-11.42 \ln \frac{7.77}{r} - 8.6007 \ln \frac{r}{6.77}}{0.137769077} \quad .$$

Now transform the initial conditions to cylindrical coordinates according to the equations:

a) r_o = initial particle radius = $7.27 + y_o$

b) v_o = initial particles velocity in the $r - \phi$ plane = $(v_{zo}'^{\,2} + v_{yo}^{\,2})^{\frac{1}{2}}$

c) $v_{\zeta o} = v_{xo}$

d) $\zeta_o = x_o$

e) α_o = initial angle of the v_o vector relative to the z axis, $\alpha_o = \tan^{-1} \frac{V_{yo}}{V_{zo}'}$.

The following is based on the treatment of Hughes and Rojansky [3]. The differential equation describing the orbit is:

$$h^2 \mu^2 \left(\frac{d^2\mu}{d\phi^2} + \mu\right) = \frac{Ae}{m}\,\mu$$

$\mu = \frac{1}{r}$ $\qquad$ $h = r_o\, v_o \cos \alpha_o$ = initial angular momentum

$$A = \frac{V_2 - V_1}{\ln\left(\frac{r_2}{r_1}\right)}$$

Making the substitution $y = \mu/\mu_o$:

$$\frac{d^2y}{d\phi^2} = \frac{c^2}{y} - y$$

$$c^2 = \frac{Ae}{mv_o^2\cos^2\alpha_o}$$

with the boundary conditions:

$$\phi = 0, \quad y = 1, \quad \left(\frac{dy}{d\phi}\right)_o = -\tan\alpha_o$$

The equation has the approximate solution:

g) $y = c + (1-c)\cos\sqrt{2}\,\phi - (\tan\alpha_o \sin\sqrt{2}\,\phi)/\sqrt{2}$

h) $\frac{dy}{d\phi} = -\tan\alpha = -(1-c)\sqrt{2}\sin\sqrt{2}\,\phi - \tan\alpha_o\cos\sqrt{2}\,\phi$.

At the exit of the plates, $\phi = 111.7°$

$$\cos\sqrt{2}\,\phi = -0.926972$$

$$\sin\sqrt{2}\,\phi = 0.375130 \quad .$$

Equations (g) and (h) are used to compute y_f and hence $r_f = r_o/y_f$ and $\alpha_f = -\tan^{-1}(dy/d\phi)_f$ at the analyzer exit. Since we assumed that $E_\zeta \equiv 0$, then $V_{\zeta F} = V_{\zeta o}$.

Now we have V_f, r_f, α_f, $V_{\zeta f}$. Define a new cartesian coordinate system at the analyzer exit with $Z = 0$ at the exit plane. The transformation is:

$$V_{zo} = V_o\cos\alpha_f$$

$$V_{yo} = V_o\sin\alpha_f$$

$$V_{xo} = V_{\zeta f} = V_{\zeta o}$$

$$X_o = X_o \text{ (at entrance)} + V_{\zeta o}\, t_p$$

$$Y_o = r - 7.27$$

$$Z_o = 0 \quad .$$

The transit time t_p through the plates can be approximated by:

$$t_p = \frac{\text{path length}}{V_o} = \frac{14.173}{V_o} \quad .$$

As the particle leaves the plates, there is a refraction due to the jump in potential from $\phi(r_f)$ to $\phi_1 = -10.0069$ statvolts. Hence as before, compute a new V_{zo} according to:

$$V_{zo}' = \left[\frac{2e}{m}(\phi(r_f) - \phi_1) + V_{zo}^2\right]^{\frac{1}{2}} \quad .$$

10) Between the exit of the plates and the plane of ED1 and ED2, the particle is in a field-free region. The equations of motion are:

a) $X_F = X_o + V_{xo}\, t$

b) $Y_F = Y_o + V_{yo}\, t$

c) $Z_F = Z_o + V_{zo}\, t$

d) $Z_o = 0;\ Z_F = 1.28$ cm.

Solve equation (c) for t and then use (a) and (b) to compute X_F and Y_F, the final position of the particle in the plane of ED1 and ED2.

11) For ED1, the condition for a "successful" particle is that it strikes within a rectangular aperture of $\Delta x = 0.2$ cm, $\Delta y = 0.5$ cm centered at $x = -2.79$, $y = 0$. For ED2, the condition for a "successful" particle is that it strikes within a 0.319 cm diameter circle centered at $x = -3.7$ cm, $y = o$.

APPENDIX A

DEFINITIONS AND PHYSICAL CONSTANTS

E = electric field, c.g.s. units, statvolts/cm

V = particle velocity (cm/sec)

ζ_o = initial particle energy (ergs)

V_o = initial particle velocity = $\left(\frac{2\zeta_o}{m}\right)^{\frac{1}{2}}$

(To convert from energy in electron volts to energy in ergs multiply by 1.6022×10^{-12}.)

M = proton mass = 1.673×10^{-24} grams

e = electronic charge = 4.80325×10^{-10} e.s.u.

1 statvolt = 299.7925 volts

Section 9 VdeF = 423.6399 volts

For E Center = 3075 eV 3000 E.G.S. 6/23/76

$$A = \frac{V_2 - V_1}{\ln \frac{r_2}{r_1}} = 20.51419$$

$$c^2 = \frac{Ae}{m V_o^2 \cos^2 \alpha_o} = \frac{5.889706 \times 10^{15}}{V_o^2 \cos^2 \alpha_o}$$

PRECEDING PAGE BLANK NOT FILMED

PAGE 38 INTENTIONALLY BLANK

APPENDIX B

PARTICLE "SCORECARD" MATRICES

$-40.6 \leq \theta_1 \leq 3.87$

$-8^\circ \leq \theta_2 \leq 8^\circ$

1. Compute θ_1, θ_2.
2. Round off and fix according to:

$$\theta_1 = \mathrm{FIX}(\theta_1 + 41^\circ) \qquad 0 \leq \theta_1 \leq 79$$

$$\theta_2 = \mathrm{FIX}(\theta_2 + 8^\circ) \qquad 0 \leq \theta_2 \leq 15$$

Define M_{ij}

$$i = \theta_1 + 1 \qquad 1 \leq i \leq 80$$

$$y = \theta_2 + 1 \qquad 1 \leq j \leq 16$$

Then the θ windows are computed from the i, j values according to:

$$\theta_{1L} = (i - 1) - 41 = i - 42$$

$$\theta_{1U} = (i - 1) - 40 = i - 41$$

$$\theta_{2L} = (j - 1) - 8 = j - 9$$

$$\theta_{2U} = (j - 1) - 7 = j^1 - 8$$

Determine the probability distribution of $\theta_{1,2}$ in ISEE ray tracing.

$$\theta_1 = \tan^{-1} \frac{(x_1 - x_2)}{9.7}$$

X_1 is a random variable uniformly distributed over the interval $-472 \leq X_1 \leq 4.72$.

X_2 is a random variable uniformly distributed over the interval $-3.05 \leq X_2 \leq 3.05$.

PRECEDING PAGE BLANK NOT FILMED

PAGE 40 INTENTIONALLY BLANK

Define $y = X_1 - X_2$.

What is $p(y)$?

$p(y)$ can be found by a graphical technique discussed by Pfeiffer [4], Chapter 3.

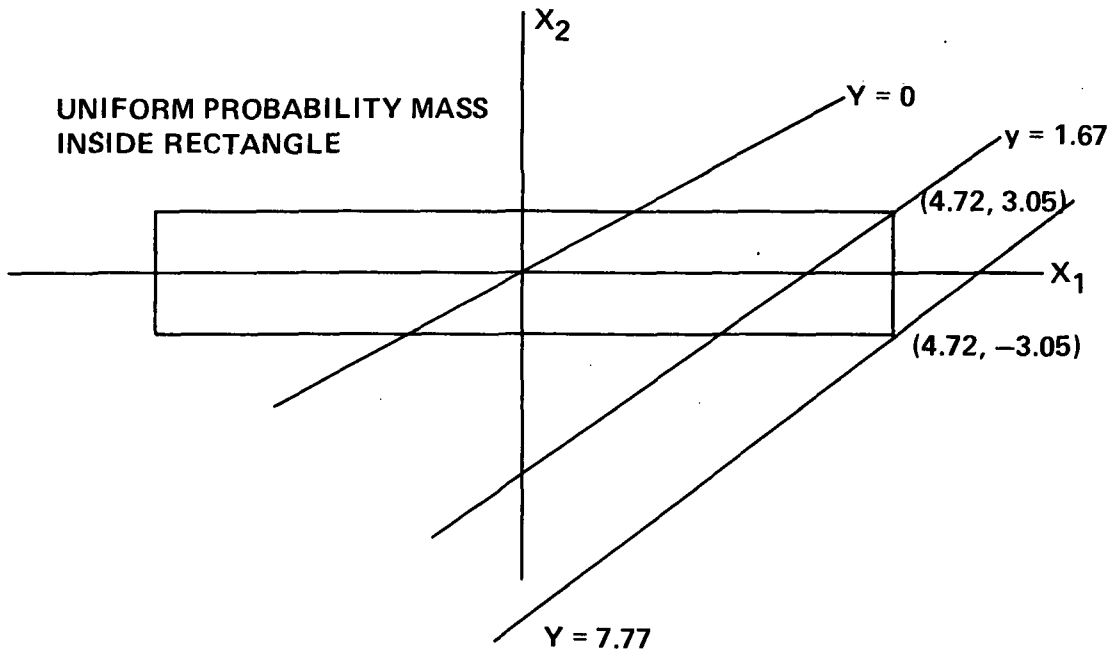

The probability density function $p(y)$ is proportional to the length of the line enclosed within the probability mass rectangle.

$$X_1 = Y - 3.05$$

$$X_2 = -Y + 4.72$$

For $1.67 \leq y \leq 7.77$

$$L = [(x_1 - 4.72)^2 + (x_2 - (-3.05))^2]^{\frac{1}{2}}$$

$$L = \sqrt{2}\,(7.77 - y) \qquad 1.67 \leq y \leq 7.77$$

$$L = \sqrt{2}\,(6.10) \qquad 0 \leq y \leq 1.67$$

Now:

$$p(x,y) = \frac{1}{\Delta x_1 \, \Delta x_2} = \frac{1}{57.584}$$

$$p(y) = \frac{L}{\sqrt{2}} \; p(x_1, y_1)$$

$$p(y) = 1.737 \times 10^{-2(7.77 - y)} \qquad 1.67 \leq y \leq 7.77$$

$$p(y) = 0.1059 \qquad 0 \leq y \leq 1.67$$

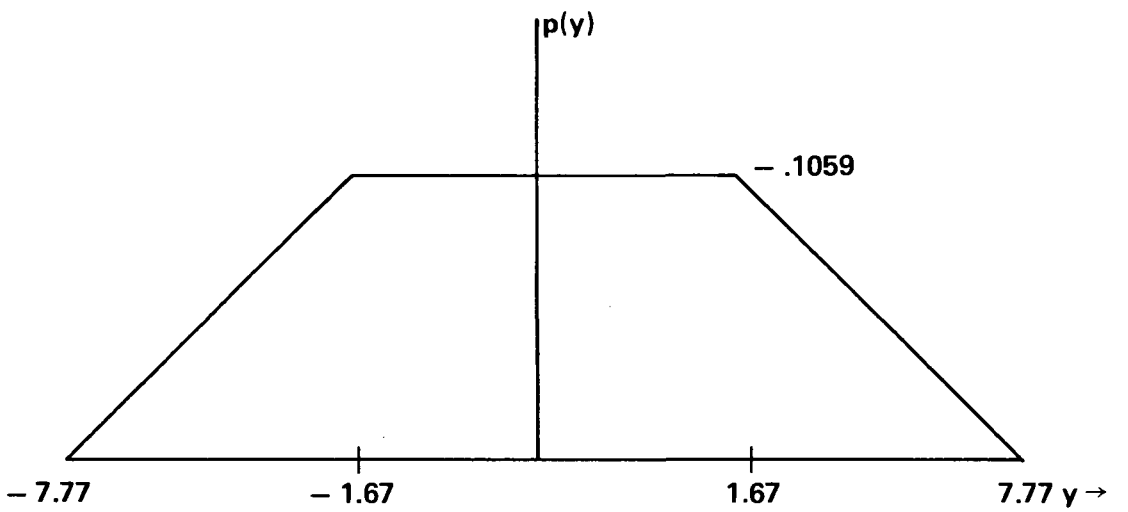

Now:

$$\theta_1 = \tan^{-1} \frac{y}{9.7}$$

$$p(\theta_1) = \frac{p(y)}{d\theta/dy} = p(y) \; 9.7 \; (1 + \tan^2\theta_1)$$

$$p(\theta) = p(y = 9.7 \tan \theta_1) \; 9.7 \; (1 + \tan^2\theta_1)$$

For $-3.87° \leq \theta \leq 38.7°$

$$p(\theta_1) = 0 \quad \text{for} \quad |\theta_1| > 38.7°$$

In a similar manner we can compute $p(\theta_2)$.

Define $Z = Y_1 - Y_2$.

Y_1 is r.v. uniform over $-1.1 \leq y \leq 1.1$

Y_2 is r.v. uniform over $-2.63 \leq y_2 \leq 0.263$

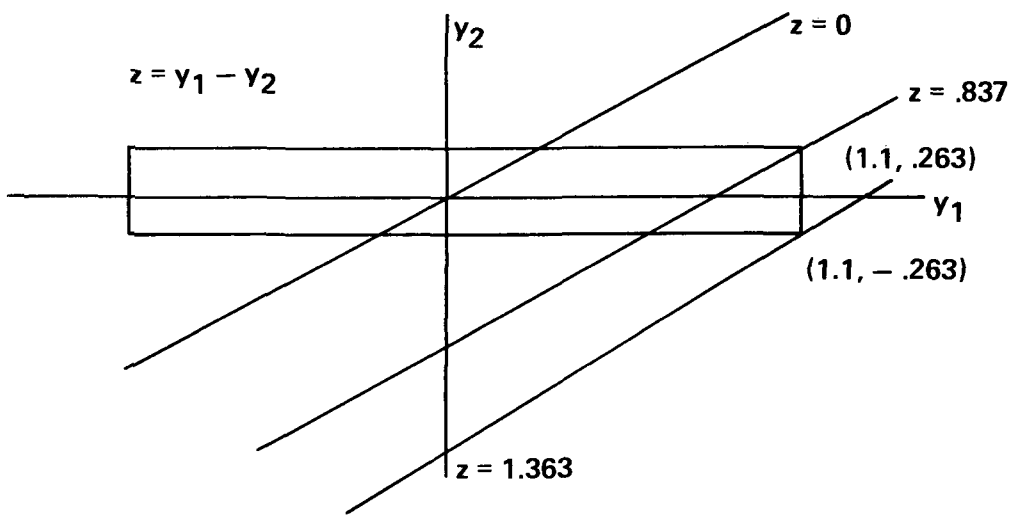

$$\left.\begin{aligned} y_1 &= z - 0.263 \\ y_2 &= -z + 1.1 \end{aligned}\right\} \quad \text{for } 0.837 \leq z \leq 1.363$$

$$L = [(y_1 - 1.1)^2 + (y_2 - (-0.263))^2]^{\frac{1}{2}}$$

$$= [(z - 1.363)^2 + (-z + 1.363)]^{\frac{1}{2}}$$

$$L = \sqrt{2}\,(1.363 - z) \qquad \text{For } 0.837 \leq z \leq 1.363$$

$$L = \sqrt{2}\,(0.526) \qquad \text{For } 0 \leq z \leq 0.037$$

$$p(z) = \frac{L}{\sqrt{2}} \; \frac{1}{1.1572}$$

$$p(z) = 0.864\,(1.363 - z) \qquad 0.837 \leq z \leq 1.363$$

$$= 0.455 \qquad 0 \leq z \leq 0.837$$

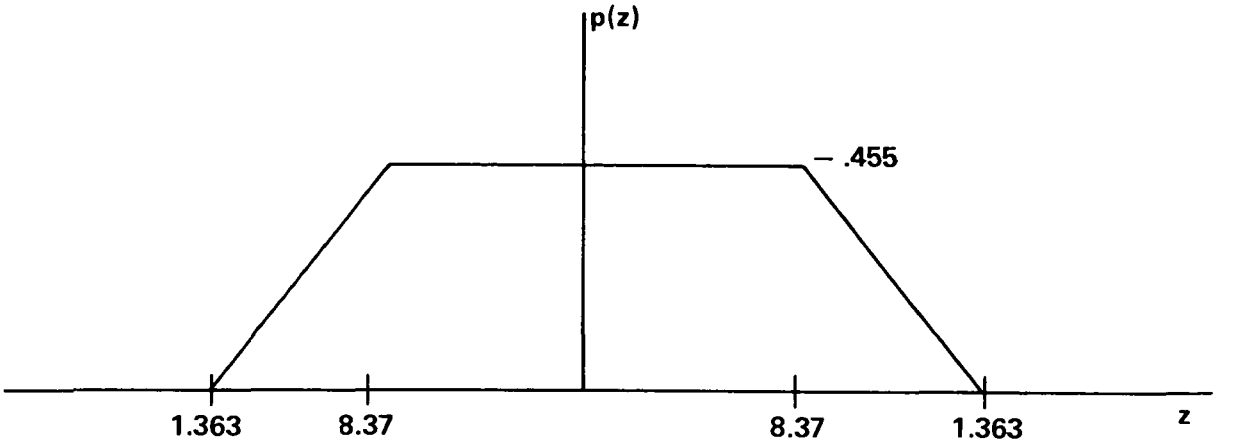

$$\theta_2 = \tan^{-1} \frac{z}{9.7}$$

$$p(\theta_2) = p(Z - 9.7 \tan \theta_2)\ 9.7\ (1 + \tan^2 \theta_2)$$

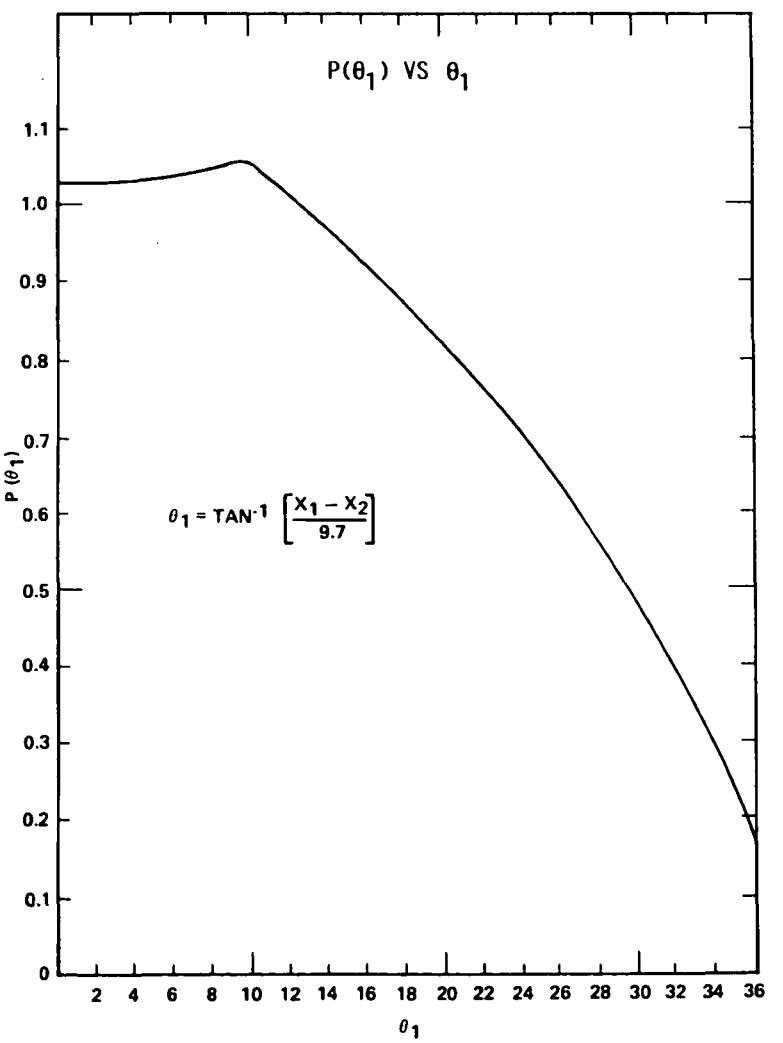

Figure 25. Probability response as a function of theta 1.

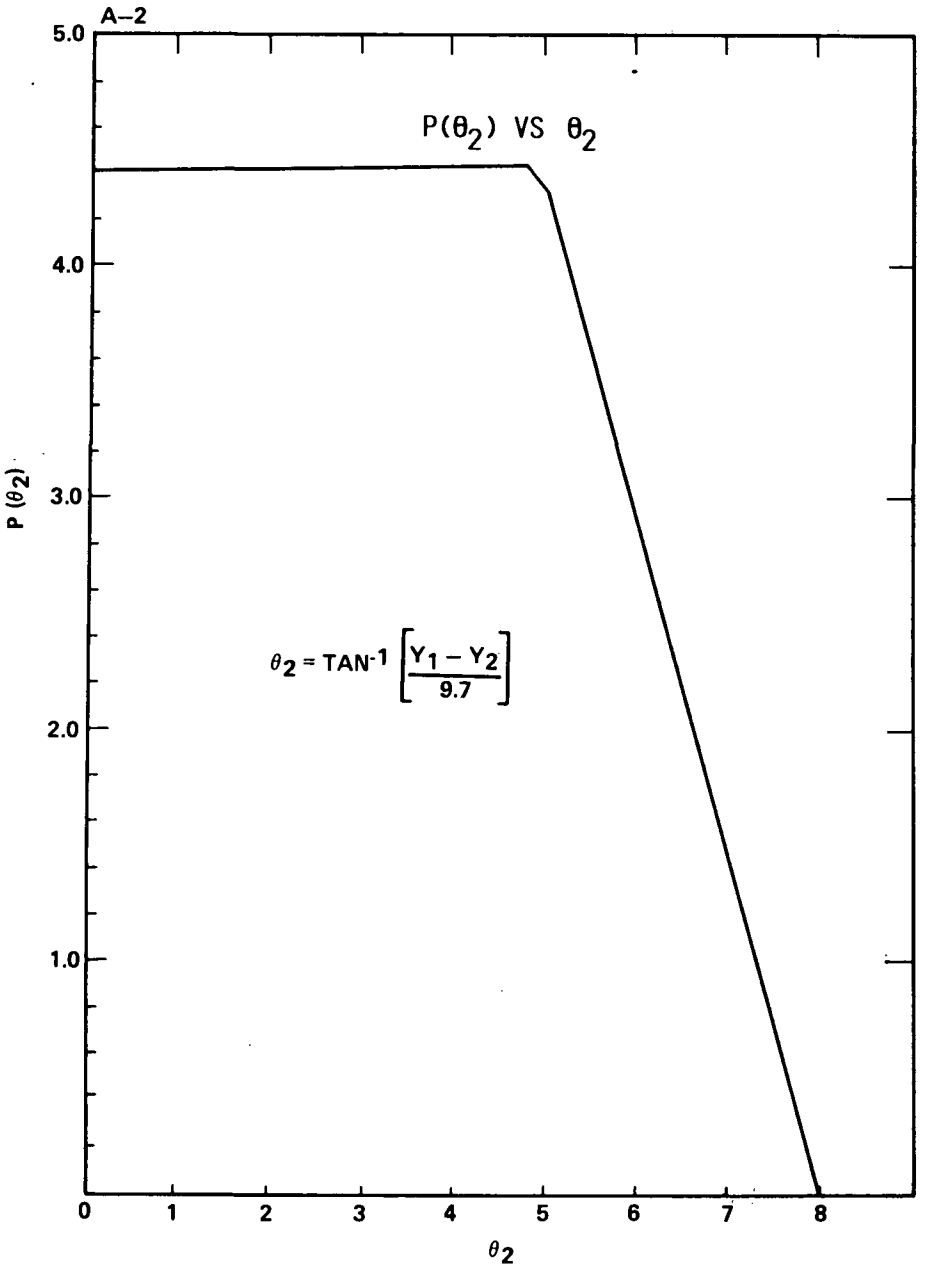

Figure 26. Probability response as a function of theta 2.

APPENDIX C

COMPUTATION OF GEOMETRIC FACTOR (G.F.) FROM THE DATA

$$G.F. \overset{\text{def}}{=} \int A(\Omega)\,d\Omega = \int A(\theta_1, \theta_2)\, d\theta_1, d\theta_2$$

In the ray-tracing method used here, the detector aperture is effectively the grid B2. The entrance aperture serves only to limit the incoming particles in angle.

If we approximate the particles in a 1° x 1° block in θ_1, θ_2 space as a unidirectional beam, then

$$A(\theta_1, \theta_2) = \frac{\text{counting rate (\#/sec)}}{\text{flux (\#/cm}^2\text{ - sec)}}$$

Define:

H_{ij} = Number of successful particles at angle θ_{1i}, θ_{2j} .

T_{ij} = Number of trials at angle θ_{1i}, θ_{2j} .

Now since B2 is uniformly illuminated with particles at constant θ_1, θ_2 (X_2, Y_2 has uniform joint probability mass over B2), then

$$\text{"}F_{ij}\text{"}(\#/\text{cm}^2) = \frac{T_{ij}}{A(B2)}$$

$$\text{"counting rate"}(\#) = H_{ij}$$

Therefore,

$$G.F. = \Delta\theta_1\, \Delta\theta_2\, A(B2) \sum_{i,j} \frac{H_{ij}}{T_{ij}}$$

$$G.F. = \frac{1}{57.3} \times \frac{1}{57.3} \times 3.49 \sum_{i,j} \frac{H_{ij}}{T_{ij}}$$

$$= 1.0631 \times 10^{-3} \sum_{i,j} \frac{H_{ij}}{T_{ij}} \quad .$$

APPENDIX D

TRAJECTORY THROUGH PLATES

Cylindrical Electric Field

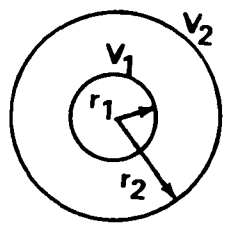

By Gauss' Thm.

$$E_r = \frac{K}{r}$$

$$\int_{r_1}^{v_2} E(r)\, dr = v_1 - v_2$$

$$K \ln \frac{r_2}{r_1} = v_1 - v_2$$

$$E_r = \frac{v_1 - v_2}{\ln \frac{r_2}{r_1}\, r} = -\frac{1}{r}\left(\frac{v_2 - v_1}{\ln\left(\frac{r_2}{r_1}\right)}\right)$$

The DE of the orbit is:

$$h^2 \mu^2 \left(\frac{d^2\mu}{d\phi^2}\right) = \frac{Ae}{m}\, \mu$$

where $\mu = 1/r$; $h = r_o v_o \cos\alpha$, $A = \dfrac{v_2 - v_1}{\ln\left(\frac{r_2}{r_1}\right)}$

This can be transformed into:

$$\frac{d^2y}{d\phi^2} + y = \frac{C^2}{y}\ ; \text{ where } C \geq \frac{Ae}{mv_o^2}$$

where the b.c. at $\phi = 0$, $y = 1$, $dy/d\phi = -\tan\alpha$.

This equation has the approximate solution:

PRECEDING PAGE BLANK NOT FILMED

PAGE 48 INTENTIONALLY BLANK

$$y = C + (1 - C) \cos (2)^{\frac{1}{2}} \phi - (\tan \alpha \sin \sqrt{2}\, \phi)/\sqrt{2} \quad .$$

At the entrance, $\phi = 0$ at $y = 1$.

At the exit, $\phi = 111.7°$,

$$\cos \sqrt{2\phi} = -0.92697$$

$$\sin \sqrt{2\phi} = 0.37513 \quad .$$

Now, the condition for a particle to be in a circular orbit is:

$$\frac{MV_o^2}{r} = \underline{Ee} = \frac{Ae}{r}$$

Hence, if $C^2 = Ae/MV_o2$, then $C < 1 \rightarrow$ the particle energy exceeds the circular orbit energy and $C > 1 \rightarrow$ the particle energy is less than the circular orbit energy.

Example: suppose $C < 1$, $\alpha = 0$.

Then $y_\theta = C - 92697\ (1-C)$

$= C(1 + 0.92697) - 0.92697 < 1$

But since $y = r_o/r$, $\rightarrow r > r_o$ at the exit.

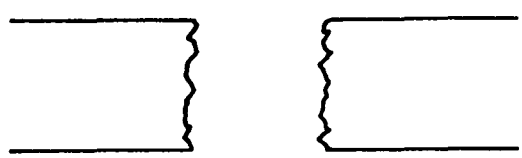

So at the analyzer entrance, we know $y = 1$, r_o, α.

At the analyzer exit, we can compute y and hence r and

$$\frac{dy}{d\phi} = -(1-C)\ \sqrt{2} \sin \sqrt{2}\ \phi - \frac{\tan\alpha}{\sqrt{2}} \sqrt{2} \cos \sqrt{2}\ \phi$$

which is equal to $-\tan\alpha$ at the exit.

APPENDIX E

EFFECTS OF REFRACTION AT ANALYZER ENTRANCE AND EXIT

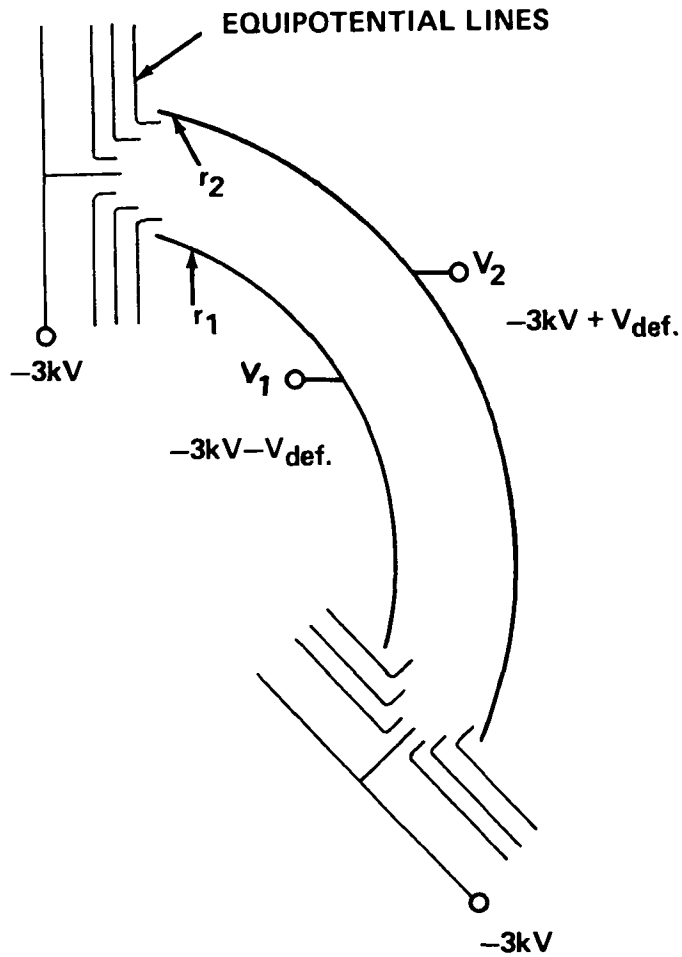

$$E_r = -\frac{1}{r} \frac{(v_2 - v_1)}{\ln \frac{r_2}{r_1}}$$

$$\phi = V_1 - \int_{r_1}^{r} E_r d_r = v_1 + \frac{(v_2 - v_1)}{\ln \frac{r_2}{r_1}} \int_{r_1}^{r} \frac{d_r}{r}$$

$$= V_1 + \frac{(v_2 - v_1)}{\ln r_2 - \ln r_1} [\ln r - \ln r_1]$$

$$= \frac{v_1 \ln \frac{r_2}{r_1} + (v_2 - v_1) \ln \frac{r}{r_1}}{\ln \frac{r_2}{r_1}}$$

$$= \frac{v_1 \ln \frac{r_2}{r} + v_2 \ln \frac{r}{r_1}}{\ln \frac{r_2}{r_1}}$$

$v_1 = -3kV - V_{def}$ $\qquad$ $V_{def} = 423.64$

$v_2 = -3kV + V_{def}$

$V_1 = -3423.64$ volts $= -11.4200$ statvolts

$v_2 = -2576.36$ volts $= -8.59381$ statvolts

$-3kV = 10.0069$ statvolts

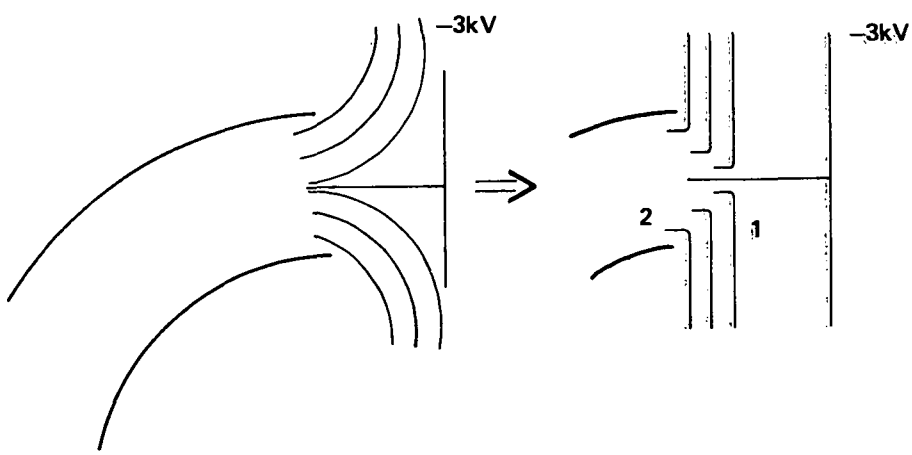

For particle in region 1

$v_z = v_{oz}$

For particle in region 2

$$1/2\ mv_{z1}^2 + q\phi_1 = 1/2\ mv_{z2}^2 + q\phi_2$$

$$v_{z2} = \left[\frac{2}{m}(q\phi_1 - q\phi_2) + v_{z1}^2\right]^{\frac{1}{2}} \qquad \phi_1 = -10.0069$$

$$\phi_2 = \frac{-11.42 \ln \frac{7.77}{r} - 8.59381 \ln \frac{r}{6.77}}{0.137769077}$$

$$r = 7.27 + y_o$$

At $r = 7.27$ $\qquad \phi_2 = -9.9582733$ statvolts

$= 0.2985.42$ volts

$$v_{z1} = 7.674 \times 10^7$$

$$v_{z2} = 7.656 \times 10^7 \quad .$$

In the analyzer plates:

$$\phi(r) = \frac{V_1 \ln \frac{r_2}{r} + V_2 \ln \frac{r}{r_2}}{\ln \frac{r_2}{r_1}}$$

$r_1 = 6.77$; $r_2 = 7.77$

$V_1 = -3$ kV $- V_{def} = -3423.64$ volts $= -11.420$ statvolts

$V_2 = -3$ kV $+ V_{def} = -2576.36$ volts $= -8.59381$ statvolts

-3 kV $= -10.0069$ statvolts

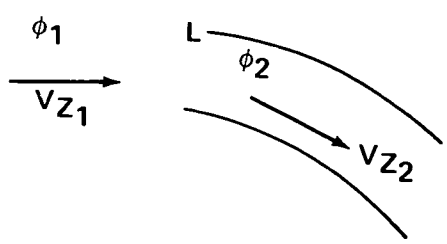

There will be a potential step function at the analyzer entrance and this step function affects only the z-component of the velocity, i.e., there is a refraction of the particle trajectory. Conservation of energy:

$$1/2\ mv_{z1}^{2} + e\phi_1 = 1/2\ mv_{z2}^{2} + e\phi_2$$

$$V_{z2} = \left[2\,\frac{e}{m}\,(\phi_1 - \phi_2) + V_{z1}^{2}\right]^{\frac{1}{2}}$$

where

$$\phi_1 = -10.0069 \text{ statvolts}$$

$$\phi_2 = \frac{-11.42 \ln \frac{7.77}{r} - 8.59381 \ln \frac{r}{6.77}}{0.137769077}$$

Algorithms:

A. Entrance of Analyzer Plates

1. Compute x_o, y_o, v_{xo}, v_{zo} at analyzer entrance as before (line 295).
2. Define $r = r_o = 7.27 + y_o$.
3. Compute v_{zo} according to equation 1 above with $v_{z1} = v_{zo}$, $v_{zo}^{1} = v_{z2}$.
4. Proceed with calculation through the plates as before.

B. Exit of Analyzer Plates

1. Compute r_1, v_{zo}, v_{yo} as before (line 318).
2. Define $r = r_1$ (line 315).
3. Compute v_{zo}^{1} according to equation 1 above with $v_{z1} = v_{zo}^{1} = v_{z2}$.
4. Proceed as before to trace particles back to detectors.

REFERENCES

1. Singh, N. and Baugher, C. R.: Sheath Effects on Current Collection by Particle Detectors with Narrow Acceptance Angles. Space Sci. Instrum., Vol. 5, 1981, p. 295.

2. Comfort, R. H., Baugher, C. R., and Chappell, C. R.: Use of the Thin Sheath Approximation for Obtaining Ion Temperatures from the ISEE 1 Limited Aperture RPA. J. Geophys. Res., Vol. 87, 1982, pp. 5109-5123.

3. Hughes, A. L. and Rojansky, V.: Phys. Rev., Vol. 34, 1929, p. 284.

4. Pfeiffer, Paul E.: Concepts of Probability. Published by McGraw-Hill Book Company, New York, New York, 1965.

APPROVAL

CALIBRATION OF THE ISEE PLASMA COMPOSITION EXPERIMENT

By C. R. Baugher, R. C. Olsen, and D. L. Reasoner

The information in this report has been reviewed for technical content. Review of any information concerning Department of Defense or nuclear energy activities or programs has been made by the MSFC Security Classification Officer. This report, in its entirety, has been determined to be unclassified.

A. J. DESSLER
Director, Space Science Laboratory

☆U. S. GOVERNMENT PRINTING OFFICE 1986—631-058/20104